(c) On the other hand, Solomon noted that in Cu(II) hydroperoxide complexes, $HO_2^- \rightarrow$ Cu(II) charge transfer transitions are observed at higher energies (340–500 nm) due to strong stabilization of π_σ^* by proton.

(d) Finally, the fact that the reduced T3 site in deoxy T2D laccase does not react with dioxygen indicates a major role for the T2 site in this reaction

Thus, it is proposed that a μ-1,1 hydroperoxide bridges one of the oxidized T3 coppers and the reduced T2 copper in the T1 Hg laccase dioxygen intermediate

- Solomon & students have also followed the formation of the 3 electron-reduced oxygen radical (2nd intermediate) in the case of native laccase using rapid kinetics. This intermediate

  (a) is formed with 2nd order rate constant of $1.7 \times 10^6\ M^{-1}s^{-1}$

  (b) has oxidized T1 center and oxidized T3 coppers (EPR, 600 nm)

  (c) exhibits no T2 EPR

  (d) shows an unusual EPR signal at $g_{eff} \sim 1.9$ at liquid Helium temperatures, which broadens when the intermediate is generated with $^{17}O_2$ (^{17}O superhyperfine interaction!)

Thus the characterization of this intermediate as a $Cu^{1+}T2\ Cu^{2+}\text{—}O\text{—}H\ Cu^{2+}T3$ associated "oxygen radical"

Multicopper Oxidases

(2) Ascorbate oxidase (squash or cucumbers)

MW 145 kDa ($\alpha_2 \beta_2$)

α 39 kDa

β 28 kDa

} two T1 copper centers
two T2 copper centers
two T3 copper centers

RX :

L-ascorbate ⟶ dehydroascorbate

O_2 + 4 H^+ ⟶ $2H_2O$

Crystal structure : (a) A. Messerschmidt, A. Rossi, R. Ladenstein, R. Huber, M. Bolognesi, G. Gatti, A. Marchesini, R. Petruzzelli, A. Finazzi-Agró, J. Mol. Biol. (1989) 206, 513-529; (b) A. Messerschmidt and R. Huber, Eur. J. Biochem. (1990) 187, 341-352. ← oxidized protein

reduced protein : crystal structure to appear soon!

Shows | T2 Cu T3 Cu_α-Cu_β trinuclear copper cluster | but there is no bridging ligand between T2 and T3 sites

Cu^{2+} T2

| 4 Å

Cu_α^{2+} — Cu_β^{2+}

3.5 Å

} T3 cluster quite similar to binuclear cluster in hemocyanin. Molecular basis for the difference in dioxygen reactivity is thus

(3) Ceruloplasmin (human blood plasma)

accounts for 90–95% of serum copper

130 kDa (MW)

2 T2 center
1 T2
1 T3 copper cluster

Function still unclear, but diverse

(a) oxidizes Fe (II)

(b) oxidizes many aromatic amines + phenols

(c) copper transport in blood?

March 9, 1993

Hemes and heme proteins

Examples:

Myoglobin (Mb)
Hemoglobin (Hb)
} O_2 - carrier

Cytochrome c
Cytochrome b_5
Cytochrome f
} electron carrier

Cytochrome c Peroxidase (CcP)
Horse-radish Peroxidase (HRP)
} Peroxidase

$$2e^- + 2H^+ + H_2O_2 \longrightarrow 2H_2O$$

Cytochrome P_{450} } Monooxygenase

$$2e^- + R-H + O_2 + 2H^+ \longrightarrow R-OH + H_2O$$

Cytochrome aa_3 and bo oxidases
Cytochrome d
} Oxidases

$$4e^- + 4H^+ + O_2 \longrightarrow 2H_2O$$

Prosthetic groups (heme)

Heme A : cytochrome aa_3 oxidases (2 heme A's)

Heme B : Mb; Hb; Cytochrome b_5; Cytochrome f; CcP; HRP; Cytochrome P_{450} [1 heme B]

Heme B (continued): Cytochrome $\underline{b}_{\underline{o}}$ (1 heme B);
Cytochrome $\underline{d}$ (2 heme B's;
called $\underline{b}_{568}$ & $\underline{b}_{595}$)

Heme O: Cytochrome $\underline{b}_{\underline{o}}$ (1 heme O)

Heme C: Cytochrome $\underline{c}$ (1 heme C)

Chlorin: Cytochrome d (1 chlorin called $\underline{d}_{650}$)

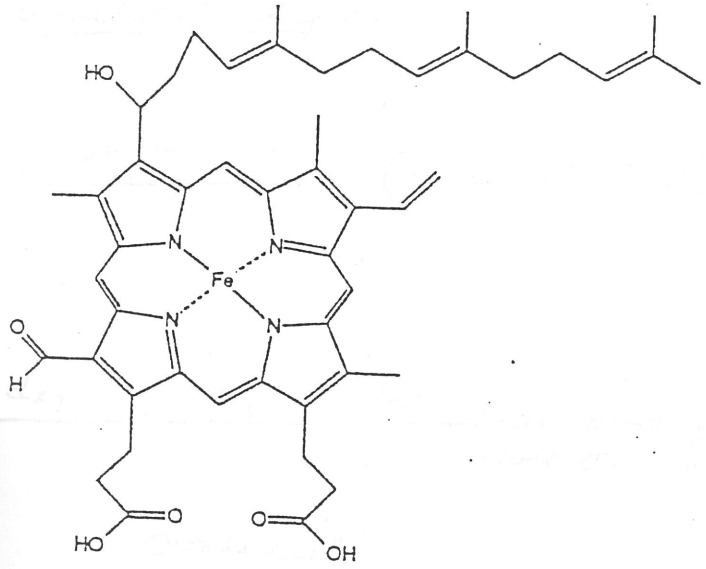

Heme A

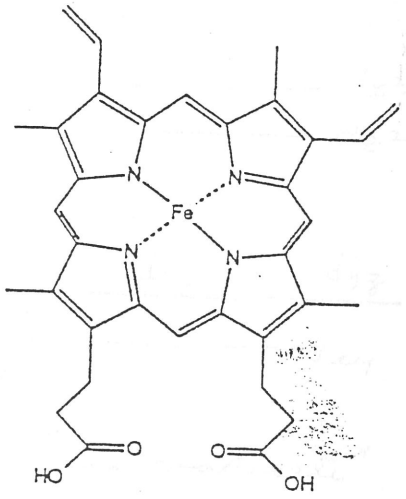

Heme B

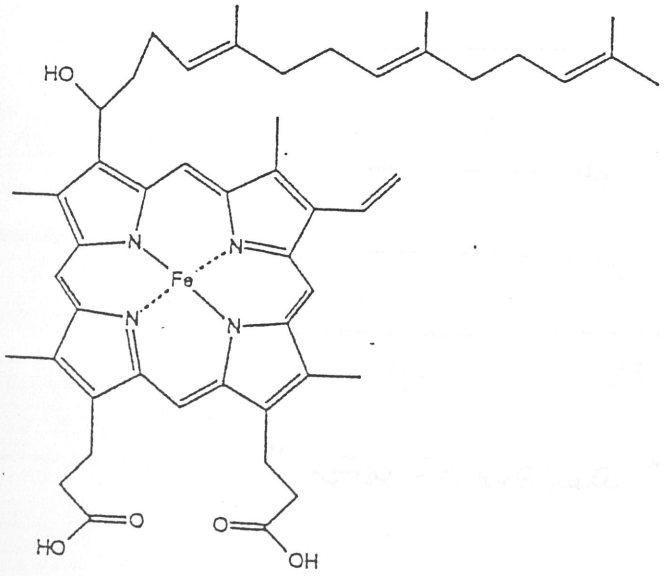

Heme O

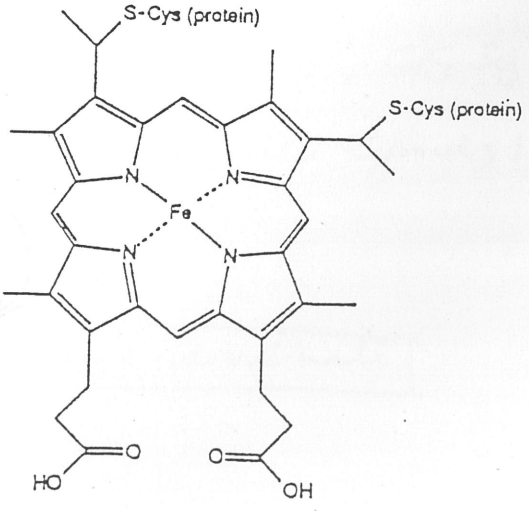

Heme C

Electronic Structure of iron porphyrins

2 parts to the problem a) Fe
b) π-system of porphyrin

[interaction between metal and porphyrin not very strong]

a) Fe

oxidation state: Fe^{2+}, Fe^{3+}, Fe^{4+}

coordination: five and six coordinate

d-orbital diagram

$d_{x^2-y^2}$ d_{z^2} (σ-antibonding)

d_{xy} d_{xz} d_{yz} (non-bonding wrt σ-bonding)

"Octahedral"

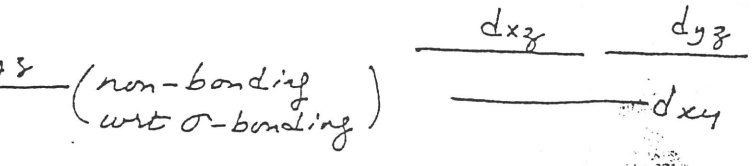

"Six-coordinate"

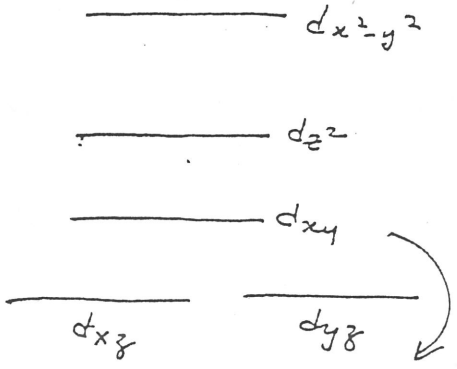

"Five-coordinate"

Iron porphyrins have a well-developed coordination Chemistry; Systematic study of the X-ray crystal structures of a large number of iron porphyrin models has revealed a coherent pattern of spin-state stereochemical relationships. (Ref. W. Robert Scheidt and Christopher A. Reed, Chem. Rev. 81, 543-555 (1981))

For example

- 4 major structural classes of iron (III) porphyrins

$[Fe(TPP)L_2]X$ ⟵ L — $Fe(TPP)X$

low spin — high spin

L = HIm, py, CN^-, 2-MeIm (strong field ligands)

$X = Cl^-, N_3^-$ (moderate field ligands)

$Fe(TPP)X \xrightarrow{AgY}$

$[Fe(TPP)L'_2]Y$ ⟵ L' — $Fe(TPP)Y$

admixed intermediate spin

$L' = R_2SO, H_2O, ROH$

weak field ligands

$Y = ClO_4^-, BF_4^-, CF_3SO_3^-$

(weak field ligands)

six coordinate — five-coordinate

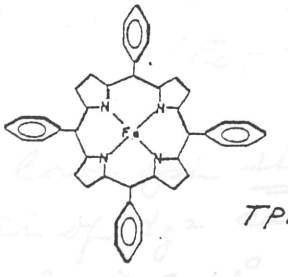

TPP ≡ meso-tetraphenylporphinatoiron

→ The ferric ion in porphinato iron (III) complexes is invariably found to have one or two axial ligands, and the complexes have tetragonal symmetry (or nearly so).

→ The five d-electrons of the ferric ion can be formally arranged into 3 possible spin states

low spin $S = 1/2$
intermediate spin $S = 3/2$ $(d_{xy})^2 (d_{xz}, d_{yz})^3 (d_{z^2})^1 (d_{x^2-y^2})^1$
high spin $S = 5/2$

→ For the intermediate spin state, there is also the possibility of spin-orbit coupling to a nearly $S = 5/2$ state to give a new quantum mechanically admixed $S = 3/2, 5/2$ state

→ Spin-state and stereochemistry of the iron (III) center is controlled almost entirely by the nature and number of axial ligands

Coordination of strong field ligands ⟶ low-spin 6-coordinate hemes e.g. bis(imidazole)

weaker field ligands ⟶ high spin 5-coordinate hemes
Cl^-, N_3^-

→ Stereochemical consequences depend on whether or not the antibonding d orbitals, $d_{x^2-y^2}$ and d_{z^2} are occupied.

Occupation of $d_{x^2-y^2}$ in a high-spin derivative ⟶ an expanded porphinato core in six-coordinate complexes ($Fe-N_p \sim 2.05\text{Å}$) or extrusion of iron atom out of the porphinato plane in five-coordinate complexes ($Fe-Ctp \sim 0.5\text{Å}$, $Fe-N_p = 2.069\text{Å}$)

low-spin derivatives
$Fe-N_p = 1.99\text{Å}$

→ When high-spin and low-spin six-coordinate complexes are compared, occupation of d_{z^2} causes extension of the axial iron-ligand bonds by $\geq 0.1\text{Å}$.

TABLE I. Spin-State/Stereochemical Relationships for (Porphinato)iron(III) Complexes

	low ($S = {}^1/_2$)	high ($S = {}^5/_2$)		admixed intermed. ($S = {}^3/_2, {}^5/_2$)	intermed.[f] ($S = {}^3/_2$)
d^5 configuration[a]	$\overline{\quad}\,x^2-y^2$ $\overline{\quad}\,z^2$ $\uparrow\downarrow$ $\uparrow\downarrow$ $\uparrow xz,yz$	$\uparrow x^2-y^2$ $\uparrow z^2$ $\uparrow$ $\uparrow$ $\uparrow$		$\uparrow x^2-y^2$ $\uparrow z^2$ $\uparrow$ $\uparrow$ $\uparrow\downarrow$	$\overline{\quad}\,x^2-y^2$ $\uparrow z^2$ $\uparrow$ $\uparrow$ $\uparrow\downarrow$
coord no.	6	5	or 6	5	6
examples	[Fe(TPP)(HIm)$_2$]$^+$ [11] [Fe(TPP)(PMS)$_2$]$^+$ [12] [Fe(TPP)(CN)$_2$]$^-$ [13] [Fe(proto)(1-MeIm)$_2$] [14] [Fe(TPP)(N$_3$)(Py)] [15] [Fe(TPP)(2-MeIm)$_2$]$^+$ [16] [Fe(TPP)(CN)(Py)] [17] [Fe(TPP)(NCS)(Py)] [18] [Fe(OEP)(3-ClPy)$_2$]$^+$ [19,b] [Fe(PF)(O$_2$)(1-MeIm)] [20] [Fe(PF)(O$_2$)(2-MeIm)] [21]	[Fe(meso)(OCH$_3$)] [22] [Fe(proto)(Cl)] [23] [Fe(TPP)(Cl)] [24] [Fe(TPP)]$_2$O [25] [Fe(proto)(SPhNO$_2$)] [26] [Fe(TPP)(NCS)] [27] [Fe(ODM)]$_2$O [28] [Fe(TPP)(Br)] [29] [Fe(TPP)(I)] [30] [Fe$_2$(μ-O)(FF)]·H$_2$O [31,f] [Fe(TPP)(F)] [32] [Fe(TPP)(NO$_3$)] [33,g]	[Fe(TPP)((CH$_3$)$_2$SO)$_2$]$^+$ [34] [Fe(TPP)(H$_2$O)$_2$]$^+$ [35] [Fe(OEP)(3-Cl(Py))$_2$]$^+$ [19,h]	[Fe(TPP)(OClO$_3$)] [36] [Fe(OEP)(OClO$_3$)] [37]	[Fe(TPP)C(CN)$_2$]$_n$ [34]
Fe-N$_p$, Å[c,d]	1.970 (14)-2.000 (6) [1.990]	2.060 (3)-2.087 (8) [2.069]	2.045 (8)	1.994 (29)-2.001 (5)	1.995 (3)
Fe-Ct$_p$, Å	0.0-0.11	0.39-0.62 [0.51]	0.0	0.26-0.30	0.0
Fe-Ct$_N$, Å	0.0-0.09	0.39-0.54 [0.47]	0.0	0.26-0.28	0.0
Ct$_N$-N$_p$, Å	1.97-2.00 [1.99]	[2.015]	2.045	1.981	1.995
Fe-Ax, Å[e]	1.957 (4)-2.013 (4)	–	2.08-2.316	2.029 (4)	2.317 (3)
hemoprotein examples	cyt b_5 cyt c, c_3, etc. metHb(CN)	(P-450)$_{ox}$	MetHb(H$_2$O)	cyt c'	–

[a] In this pictorial representation of the one-electron d-orbital energy levels only the relative energies of the d_{z^2} and $d_{x^2-y^2}$ levels are known with absolute certainty. [b] At 98 K. [c] N$_p$, porphinato nitrogen atom; Ct$_N$, center of the best plane of the four N$_p$; Ct$_p$, center of the best plane of the 24-atom porphinato core; Ax, axial ligand donor atom. [d] Values given are the ranges observed in the compounds listed. The number in parentheses is the estimated standard deviation for the extreme values. The values given in square brackets are the average value for all members of the given class. [e] The Fe-Ax distance will be that appropriate for Fe-N(imidazole) when this value is available. [f] FF is a confacial biporphyrin. [g] NO_3^- binds as an unsymmetrical bidentate ligand. [h] At 293 K, high-spin component of spin mixture. [i] In addition there are two complexes, of somewhat uncertain spin state, whose structure has been reported: [Fe(TPP)(EtOH)$_2$]$^+$ [39] and [Fe(OEP)(EtOH)$_2$]$^+$ [40]. These may be admixed intermediate-spin species.

- Four major structural classes of iron(II) porphyrins

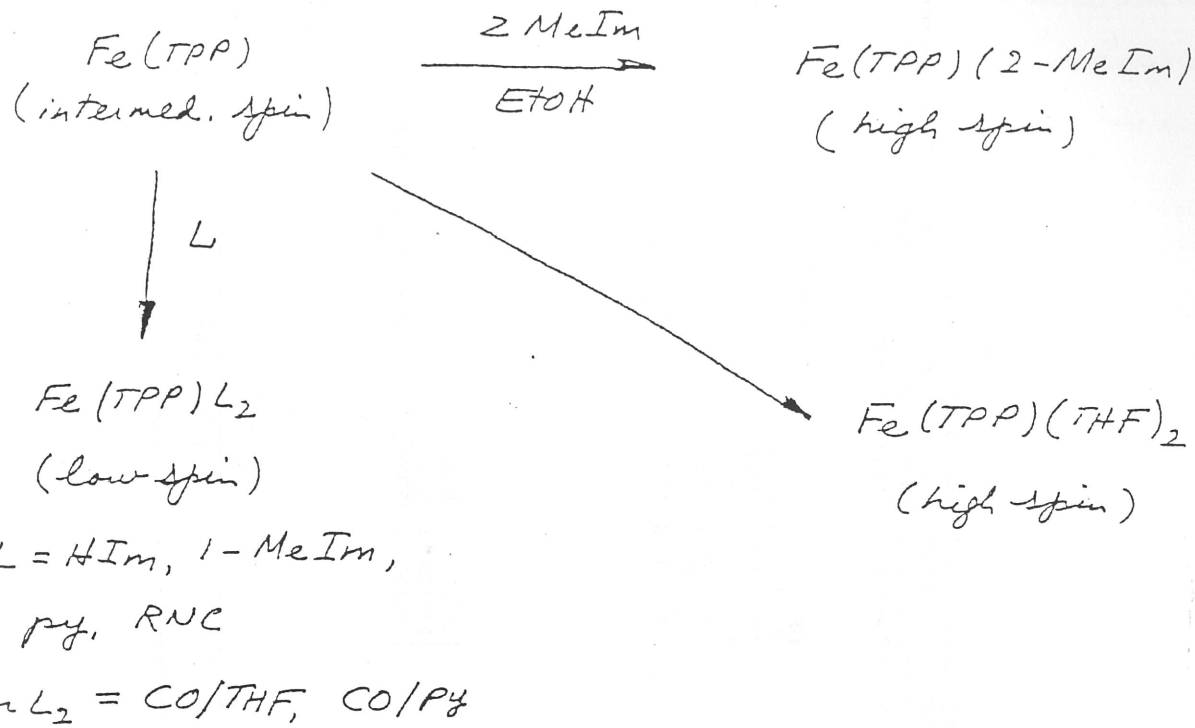

L = HIm, 1-MeIm,
py, RNC
or L_2 = CO/THF, CO/Py

→ The d^6 iron(II) can exhibit 3 spin states:

$S=0$ low spin state

$S=1$ intermediate-spin state

$S=2$ high-spin state

→ As a consequence of decreased charge, there is a small increase in radii for iron(II) compared to iron(III).
→ increased bond lengths

→ The stereochemical consequences of populating the antibonding $d_{x^2-y^2}$ and d_{z^2} orbitals are similar to those found for Fe(III), except for the following important difference: In <u>5-coordinate high-spin complexes</u>, the magnitude of the displacement of the iron(II) atom out of the plane is no larger than that of Fe(III) derivatives, despite the larger size of Fe(II). However, the Fe(II)-Np distances are

TABLE II: Spin-State/Stereochemical Relationships for (Porphinato)iron(II) Derivatives

	low ($S = 0$)		high ($S = 2$)		intermed. ($S = 1$)
d^6 configuration[a]	$\uparrow\downarrow$ $-x^2-y^2$ $-z^2$ $\uparrow\downarrow xy$ $\uparrow\downarrow xz, yz$		$\uparrow$ $\uparrow x^2-y^2$ $\uparrow z^2$ $\uparrow\downarrow xy$ $\uparrow xz, yz$		$\uparrow$ $-x^2-y^2$ $\uparrow\downarrow z^2$ $\uparrow\downarrow xy$ $\uparrow$ $\uparrow xz, yz$
coord no.	5 or	6	5 or	6	4
examples	[Fe(TPP)(NO)][44] [Fe(OEP)(CS)][46]	[Fe(TPP)(Pip)$_2$][47] [Fe(TPP)(NO)(B)][48] [Fe(TPP)(CO)(Py)][49] [Fe(Deut)(CO)(THF)][50] [Fe(TPP)(THT)$_2$][12] [Fe(TPP)(*t*-BuNC)$_2$][51] [Fe(TPP)(1-MeIm)$_2$][52] [Fe(TPP)(CO)(SR)]$^-$ [53] [Fe(TPP)(CCl_3)(H_2O)][54] [Fe(C5Im)(TPP)(THT)][12]	[Fe(TPP)(2-MeIm)][55] [Fe(TPP)(SR)]$^-$ [53] [Fe(PF)(2-MeIm)][21]	[Fe(TPP)(THF)$_2$][56]	[Fe(TPP)][57]
Fe-N_p, Å[b,c]	1.981 (4)-2.001 (3)	1.981 (29)-2.008 (12) [2.002]	2.072 (6)-2.096 (4) [2.085]	2.057 (4)	1.972 (4)
Fe-Ct_p, Å	0.21-0.23	0.0-0.10	0.43-0.62 [0.53]	0.0	0.0
Fe-Ct_N, Å	0.21-0.23	0.0-0.11	0.40-0.52 [0.45]	0.0	0.0
Ct_N-N_p, Å	1.970-1.990	[2.000]	2.030-2.044 [2.036]	2.057	1.972
Fe-Ax, Å[d]	1.717 (7)	2.014 (5)	2.095 (6)-2.161 (5)	2.351 (3)	-
hemoprotein example	Hb(NO)·DPG[59] (T-state)	Hb(CO) cyt b_5 cyt *c*, c_3, etc	Hb	Hb(H_2O) ?	-

[a] In this pictorial representation of the one-electron d-orbital energy levels only the relative energies of the d_{z^2} and $d_{x^2-y^2}$ levels are known with absolute certainty. [b] N_p, porphinato nitrogen atom; Ct_N, center of the best plane of the four N_p; Ct_p, center of the best plane of the 24-atom porphinato core; Ax, axial ligand donor atom. [c] Values given are the ranges observed in the compounds listed. The number in parentheses is the estimated standard deviation for the extreme values. The values given in square brackets are the value for all members of the given class. [d] The Fe-Ax distance will be that appropriate for Fe-N(imidazole) when this value is available.

larger (i.e., longer Fe–Np bonds), and the size of the central hole (Ct_N–Np) increases by about 0.02 Å to ≥ 2.03 Å (core expansion). The out-of-plane displacement is typically ~0.5 Å, compared to ~0.21 Å for low-spin five-coordinate Fe(TPP)NO and ≤ 0.11 Å for six-coordinate low-spin complexes.

→ As in Fe(III), it is possible to coordinate two weak-field axial ligands to yield a six-coordinate derivative, e.g. Fe(TPP)(THF)$_2$. The ferrous atom fits into the porphyrin plane, with Ct_N–Np ~ 2.057 Å, Fe–Np = 2.057 Å, representing a substantial radial core expansion of the iron porphyrin.

(b) Porphyrin

uv-visible spectra of heme arise from π–π* electronic transitions of the porphyrin. Our understanding of the electronic spectra of porphyrins and metalloporphyrins is due largely to the work of Martin Gouterman (J. Chem. Phys. 30, 1139 (1959).

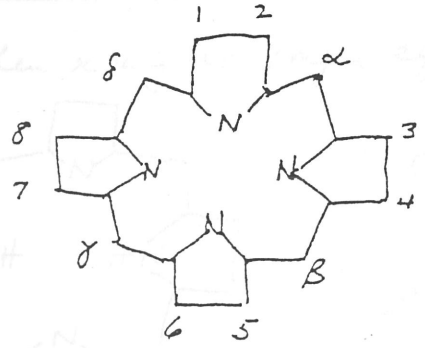

D_{4h}

22-π electrons

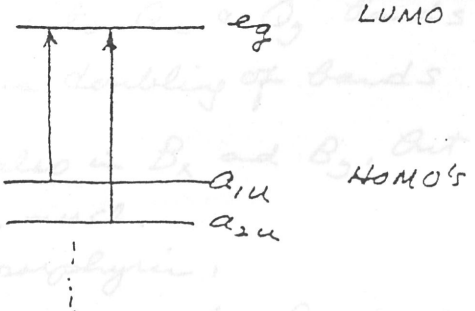

1e⁻ molecular orbitals

$\pi - \pi^*$ transitions

- $(\ldots a_{2u}^2 a_{1u}^2 e_g^0) \longrightarrow (\ldots a_{2u}^1 a_{1u}^2 e_g^1)$

  A_{1g} symmetry → E_u symmetry

  intense — B transition (Soret)

- $(\ldots a_{2u}^2 a_{1u}^2 e_g^0) \longrightarrow (\ldots a_{2u}^2 a_{1u}^1 e_g^1)$

  A_{1g} symmetry → E_u symmetry

  weak* — Q transition (α, β)

* Configuration interaction mixes these two molecular states and enhances Q bands

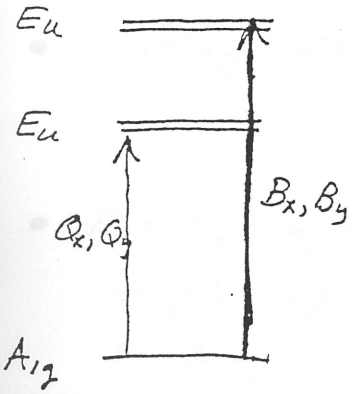

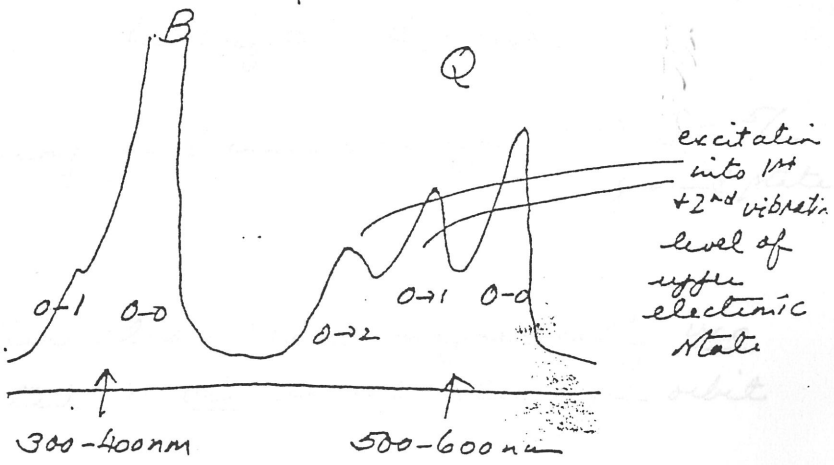

exact spectral position depends on nature of metal ion and porphyrin substituent

Deviation from D_{4h} symmetry

When x & y no longer equivalent, e.g. in free-base porphyrin,

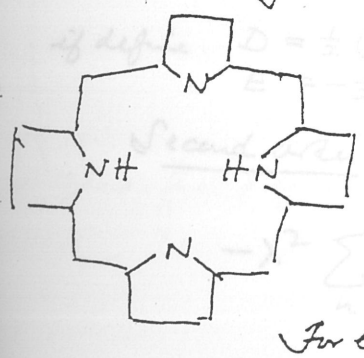

Q bands split into Q_x & Q_y bands
i.e., there is doubling of bands

B bands split also in B_x and B_y, but not affected as much.

For example, in free base porphyrin:
Q_x & Q_y split by 2960 cm^{-1} ; B_x & B_y by 240 cm^{-1}

EPR (electron paramagnetic resonance)

a) Low spin d^5 (six-coordinate Fe(III) porphyrin with strong-field axial ligands)

1 unpaired electron in d_{xz}, d_{yz} orbital

g-tensor anisotropic due to spin-orbit coupling

Effective g-values: 3, 2, 1.5

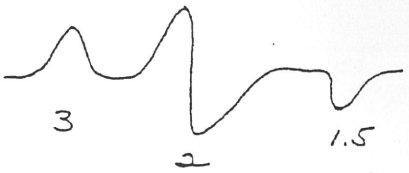

b) High spin d^5

5-unpaired electrons (d_{xy} d_{xz} d_{yz} d_{z^2} $d_{x^2-y^2}$)

- Exchange interaction among five unpaired spin $\Longrightarrow S = 5/2$ ground state

- But the unpaired electrons also interact magnetically via dipole-dipole interaction & via second-order spin orbit coupling

$$\mathcal{H}_{Dipolar} = g^2\beta^2 \sum_{i>j} \left[\frac{\vec{S}_i \cdot \vec{S}_j}{r_{ij}^3} - \frac{3(\vec{S}_i \cdot \vec{r}_{ij})(\vec{r}_{ij} \cdot \vec{S}_j)}{r_{ij}^5} \right]$$

$$\longrightarrow -X\hat{S}_x^2 - Y\hat{S}_y^2 - Z\hat{S}_z^2$$ where S_x, S_y, S_z are components of the total spin along molecular axes

$$\longrightarrow D\left(S_z^2 - \tfrac{1}{3}S(S+1)\right) + E\left(S_x^2 - S_y^2\right)$$

if define $D = \frac{1}{2}(X+Y) - Z$

$E = -\frac{1}{2}(X-Y)$

Second order spin orbit coupling has the form

$$-\lambda^2 \sum_n \frac{\int \Psi_0^* (\vec{L}\cdot\vec{S})\, \Psi_n \, d\vec{\tau} \cdot \int \Psi_n^* (\vec{L}\cdot\vec{S})\, \Psi_0 \, d\vec{\tau}}{E_n - E_0}$$

$$\longrightarrow \vec{S} \cdot \underset{\sim}{D}' \cdot \vec{S} \quad \text{where } D_{\alpha\beta} = -\lambda^2 \sum_n \frac{\int \Psi_0^* L_\alpha \Psi_n \, d\tau \cdot \int \Psi_n^* L_\beta \Psi_0 \, d\tau}{E_n - E_0}$$

can also be cast into the form

$$\longrightarrow D'\left(S_z^2 - \tfrac{1}{3}(S)(S+1)\right) + E'\left(S_x^2 - S_y^2\right)$$

So combine & give what is frequently referred to as zero-field term of Hamiltonian

$$\mathcal{H}_{\substack{\text{zero-field}\\ \text{splitting}}} = D\left(S_z^2 - \tfrac{1}{3}S(S+1)\right) + E\left(S_x^2 - S_y^2\right)$$

For Fe-porphyrin

z ⊥ porphyrin plane

x, y in porphyrin plane

$$\longrightarrow D\left(S_z^2 - \tfrac{35}{12}\right) + E\left(S_x^2 - S_y^2\right)$$

and $(S_z^2)_{av} = (m_S)^2$ where $m_S = \pm 5/2, \pm 3/2, \pm 1/2$

projection of spin along z-axis or porphyrin normal

$\frac{10}{3}D$ ═══ $\pm 5/2$

$-\frac{2}{3}D$ ═══ $\pm 3/2$

$-\frac{8}{3}D$ ═══ $\pm 1/2$

m_S

Energy levels for $E = 0$

$D \sim 2\text{–}10\ cm^{-1}$

$E \sim 0 - 0.04\ cm^{-1}$

zero-field splitting

e.g. Metmyoglobin

$D = 9\ cm^{-1}$

Metmyoglobin fluoride

$D \simeq 6\ cm^{-1}$

Conventional EPR only observed for ± ½ level,
the so-called Kramer doublet

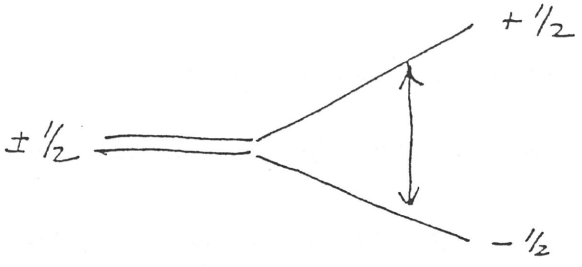

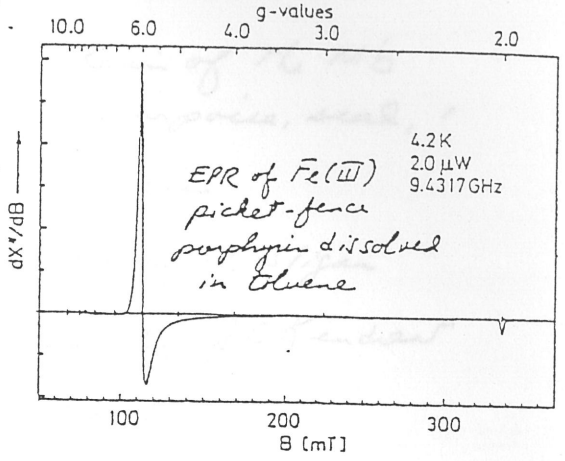

$g_{eff} \cong 2$ when $H_0 \parallel z$

6 when $H_0 \perp z$; i.e., in x-y plane.

$g_{x,y}^{eff} = 6 \pm (24 \cdot \frac{E}{D})$ for deviation from axial symmetry

Fe-porphyrin is usually undertaken near liquid helium temperature, where essentially lowest level is populated ($S_z \pm ½$ Kramer doublet if $D > 0$)

(c) <u>High-spin d^6</u>

$S = 2$ (4 unpaired electrons)

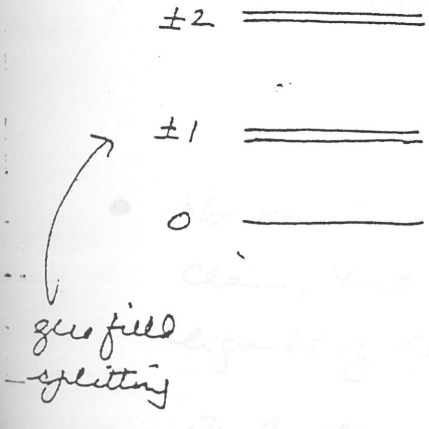

no Kramer doublet

→ no conventional EPR !

(d) Low-spin d^6

$S = 0$ no EPR !

Myoglobin

- MW 18,000 Da
molecular mass
- 153 amino acids in the polypeptide chain of the Mb from sperm whale, horse, porpoise, seal, ...
- primary sequence known for many species
- Human Mb cloned and overexpressed by P. Sligar
- X-ray crystal structure well studied by J.C. Kendrew
  (Scientific America 205, 96 (1961)
  Science 139, 1259 (1963)
- 1 proto heme IX.

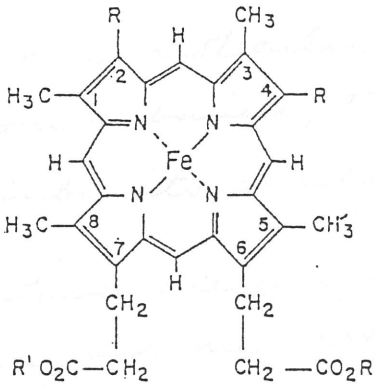

Fig. Structure of some porphyrin-iron complexes. Protoheme IX (Proto): R = $-CH=CH_2$; Deuteroheme IX (Deut): R = $-H$; Mesoheme IX (Meso): R = $-CH_2-CH_3$; Heme c: R = $-CH(CH_3)-S-$Polypeptide chain; Porphin-iron complexes: All the substituents 1 to 8 are protons. R' = $-H$ in the heme groups of myoglobin, hemoglobin, and cytochrome c.

- No covalent bonds between proto heme IX and polypeptide chain, but the histidyl residue at F-8 is one of the axial ligands of the heme iron
- The function of the sixth coordination site is to reversibly bind & release molecular oxygen when Fe is in ferrous state
- Other ligands bind to the sixth coordination site as well.

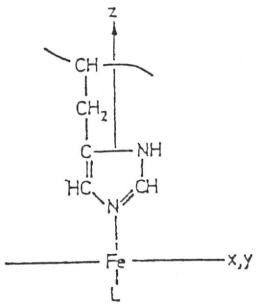

L = H_2O, CN^-, N_3^-, OH^- (Fe^{3+})
O_2, CO, NO (Fe^{2+})

- Propionic acid groups important in orienting heme VI's & VII's polypeptide fold.

Hemoglobin

- Mammalian Hb's have molecular masses of ~ 65 kDa, and consist of four subunits, two each of two types, called α and β subunits or chains.

- Each subunit contains one polypeptide chain of ca 150 amino acid residues, and one protoheme IX. Heme is attached to histidyl residue at F-8 in each subunit as is in Mb.

- The amino acid sequence is known for many Hb's from different species.

- 3-dimensional structure has been extensively studied by Max Perutz (J. Mol. Biol. 13, 646 (1965); Nature 219, 131 (1968); Nature 222, 1240 (1969).

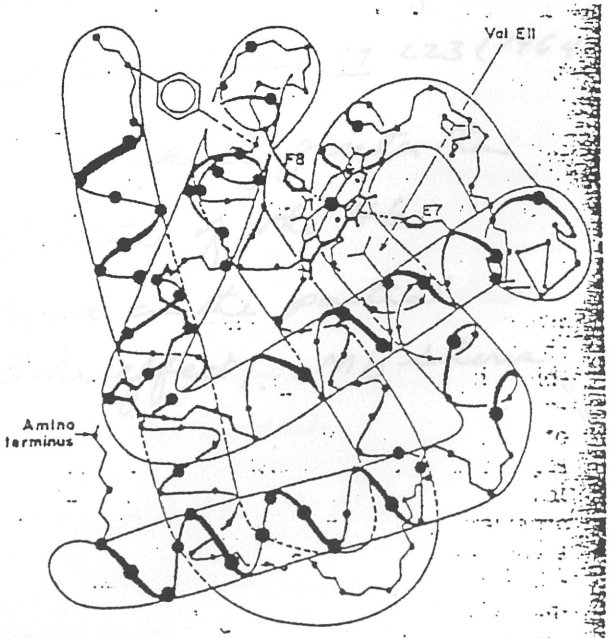

A schematic representation of one subunit of hemoglobin. The proximal histidine F8 and the distal Val-11 and distal histidine E7 are shown. This figure was adapted from a figure kindly provided by Dr. M. F. Perutz.

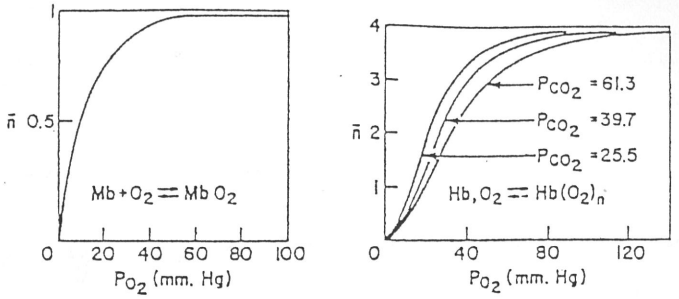

[redacted]. Oxygenation curves for myoglobin and hemoglobin. The average number of oxygen molecules bound per protein molecule, $\bar{n}$, is plotted vs. the partial pressure of O_2. For hemoglobin the oxygenation curve is given at three different partial pressures of carbon dioxide

- Each heme group of the tetrameric Hb binds dioxygen. The binding of dioxygen is cooperative, reflecting allosteric interactions between the four subunits. In above figure, the oxygenation curve for Mb has a shape expected for a bimolecular reaction. On the other hand, the oxygenation curve for Mb is sigmoidal, indicating that the affinity for oxygen of partially ligated Hb is greater than that of deoxy Hb. The free energy of the subunit interaction is ca 3 kcal/mole, which is about 10% of the total free energy for complete oxygenation of the Hb tetramer (Ref. J. Wyman, Adv. Protein Chem. 19 223 (1964),

Note that the oxygen affinity of Mb is markedly greater than that of Hb. Another interesting feature of the Hb oxygenation curve is its dependence on the partial pressure of CO_2, and on pH (Bohr effect). Mb shows no Bohr effect.

Cytochrome c

- Molecular mass of 12,500
- The sequence of the 103 to 109 amino acids of the polypeptide chain is known for ~50 different species.
- 1 heme c per molecule, covalently linked to the cysteinyl residues at positions 14 and 17 of the polypeptide chain. The two axial positions of the heme are occupied by amino acids : 1 histidyl residue and 1 methionyl residue
- Functions as an electron carrier as the heme interconverts between the Fe^{2+}/Fe^{3+} oxidation states
- 3-dimensional structures known for a number of Cytochrome c's (R. Dickerson (UCLA), and Canadian group at UBC)

Cytochrome P-450

- ubiquitous enzyme, found in plants, animals, yeast and bacteria
- a mono-oxygenase, that catalyze the oxygenation of substrates by insertion of one atom of dioxygen while the other atom is reduced to water.

$$R-H + O_2 + 2H^+ + 2e^- \longrightarrow R-OH + H_2O$$

- Substrates for the P-450 enzymes are quite diverse, ranging from alkanes and alkenes, to arenes and sulfides

- The enzymatic transformations are equally diverse, including production of alcohols, epoxides, phenols and sulfoxides
- Called P-450 because of its Soret absorption at 450 nm. Soret for the ferrous–CO derivative occurs at 420 nm.
- Most P-450 are membrane-bound. However, the P-450 from camphor-grown Pseudomonas putida (P-450-CAM) is water-soluble and has been extensively studied by physical methods. The crystal structure of this P-450 has also recently been worked out by T. Poulos. Axial ligands to heme in native enzyme: cysteine thiolate and H_2O
- All P-450 enzymes share the common reaction cycle shown below.

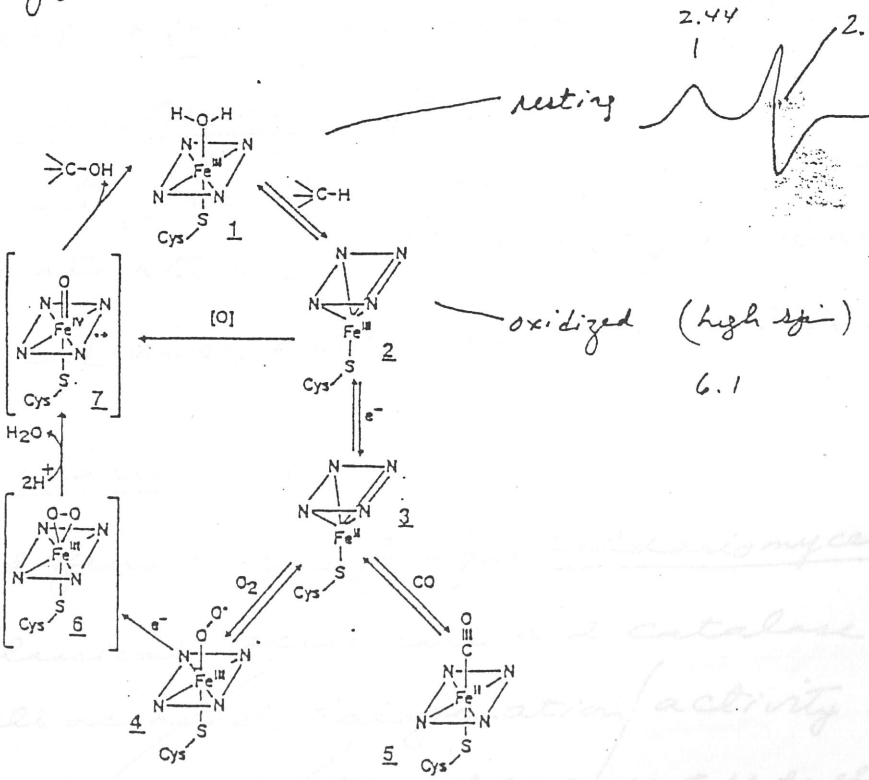

Catalytic cycle of cytochrome P-450 and the postulated partial structures of the intermediates. The dianionic porphyrin macrocycle is abbreviated as a parallelogram with nitrogens at the corners, in this and subsequent figures. Oxy-P-450 (*4*) is shown as a complex of ferric porphyrin and superoxide anion, but could also be described as an adduct of neutral dioxygen and ferrous porphyrin. States *6* and *7* are hypothetical intermediates whose structures have not been established. Structures *1*, *2*, and *7* are neutral (the dot and the positive charge on *7* indicate the radical state and electron deficiency of the π electron system of the porphyrin ring), while the overall charge on structures *3*, *4*, and *5* is minus one and on structure *6* is minus two. Adapted from Ref. [22]

(a) The cycle is initiated by substrate binding to the low-spin, hexa coordinate, native ferric form (1) of P-450, converting it to the high-spin, penta coordinate ferric complex, (2). (b) Reduction of 2 by one electron yields the high-spin, penta coordinate ferrous derivative, (3). (c) State 3 subsequently binds O_2 to form a "semi-stable" low-spin, hexa coordinate ferrous-dioxygen adduct (4).

‖ Note that States 1–4 of the P-450 cycle are isolable and well characterized.

(d) Beyond oxy P-450, it is thought that a ferric peroxide complex (5) is formed, with the input of another electron (the second). (e) A high-valent oxo-iron adduct (7) is then formed. (f) Finally, oxygen atom transfer from I to the substrate occurs to give the organic product and regenerate state 1. The last step probably follows a radical abstraction–recombination mechanism

Chloroperoxidase

- isolated from marine fungus Caldariomyces fumago
- has "classical" peroxidase and catalase activities as well as novel halogenation activity.

oxidation of substrates with concurrent reduction to H_2O

disproportionation H_2O_2 to $H_2O + O_2$

$$AH + X^- + H^+ + H_2O_2 \longrightarrow AX + 2H_2O$$

where $X^- = Cl^-, Br^-, I^-$

- As for P-450, axial ligand is thiolate from a cysteine

- Proposed mechanism of catalytic cycle

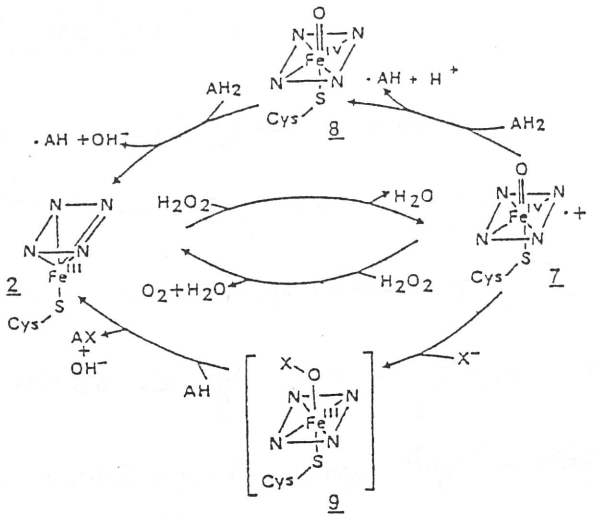

[redacted]. Catalytic cycle of chloroperoxidase and the postulated structures of intermediates. The structures of the intermediates in the peroxidase ($2 \rightarrow 7 \rightarrow 8 \rightarrow 2$) and catalase ($2 \rightarrow 7 \rightarrow 2$) modes have been partially characterized. The structure of intermediate *9* in the halogenation mode ($2 \rightarrow 7 \rightarrow 9 \rightarrow 2$) is hypothetical. Structures *2* and *7* are neutral (the dot and the positive charge on *7* indicate the radical state and electron deficiency of the π electron system of the porphyrin ring), while the overall charge on structures *8* and *9* is minus one. Adapted from Ref. [22]

The catalytic cycle of chloroperoxidase begins at state 2 (the high-spin, pentacoordinate ferric enzyme). It goes directly to state 7 upon the addition of H_2O_2 and other oxygen atom donors. Three reactivity paths are available, depending on the nature of the substrate and the presence or absence of a halogen donor.

Peroxidase mode: state 7 is reduced in two separate 1-electron steps (with concomitant substrate oxidation) to form state 8, also a high-valent oxo-iron species, and then regenerate 2

Catalase mode: state 7 carries out a two-electron oxidation of hydrogen peroxide to form O_2 and regenerate 2.

Halogenation mode : state I reacts with the halide to form a ferric hypohalite adduct (9), which then transfers an "activated" halogen to the substrate and regenerates state I

Next lecture

Horseradish peroxidase

Cytochrome c peroxidase

The electronic structure of O_2 bound to iron hemes

The details of O–O bond cleavage

Characterization of high-valent oxo-iron porphyrin systems

March 16, 1993

- Low Temperature (4.2 K) EPR is the easiest and the most unequivocal way to determine the spin state of an iron heme in the ferric state

(1) Low-spin d^5

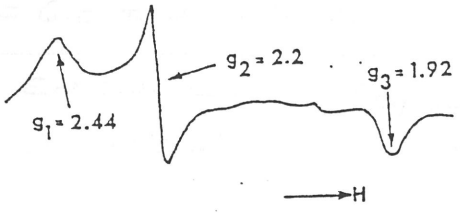

Epr of resting (oxidized) Cytochrome P-450 before substrate is bound.

(2) Other low-spin hemes in hemoproteins

g-values of low-spin hemoproteins

	g_1	g_2	g_3
Mb.OH	2.61	2.19	1.82
Mb.N_3	2.8	2.25	1.75
Hb.OH	2.6	2.3	1.7
Hb.N_3	2.82	2.2	1.70
Peroxidase.OH	2.86	2.12	1.67
Cytochrome *c* peroxidase	2.7	2.2	1.83
Cytochrome b_5	3.03	2.23	1.93
Catalase.N_3	2.80	2.18	1.74
	(2.53	2.2	1.85)
Catalase.CN	2.84	2.25	1.66
	2.56	2.31	1.81
	(2.43	2.17	1.895)

Mb is myoglobin and Hb is hemoglobin.

	g_1	g_2	g_3
Cytochrome c	3.07	2.26	1.25
Cytochrome a_3 in Cytochrome c oxidase	3.0	2.2	1.5

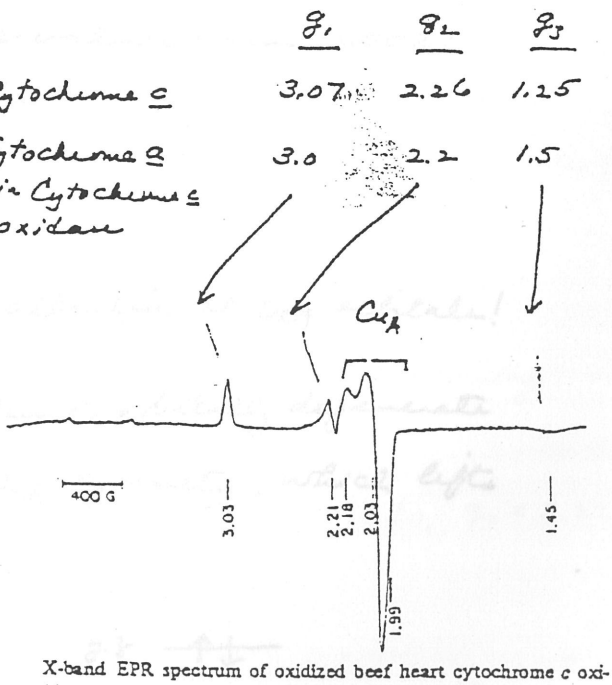

X-band EPR spectrum of oxidized beef heart cytochrome *c* oxidase at 10 K.

(3) High-spin heme centers

Hemoprotein	g_1	g_2	g_3
Met Mb	5.9		2.0
Catalase	6.6	5.4	2.0
$+F^-$	6.5	5.5	2.0
$+N_3^-$	6.7	5.2	2.0
P-450	6.6	5.3	2.0
Cytochrome a_3 in Cytochrome c oxidase	6.0		2.0

(4) Recall for high-spin heme, EPR arise from $m_S = \pm 1/2$ Kramer doublet: $\begin{cases} g \sim 6 & \text{when } \vec{H} \text{ is in porphyrin plane} \\ g \sim 2 & \text{when } \vec{H} \text{ is } \perp \text{ porphyrin plane} \end{cases}$

When porphyrin has D_{4h} symmetry (axial), $E = 0$ and $g = 6.0$. When geo-field interaction has a rhombic component, i.e., $E \neq 0$, then

$$\boxed{g = 6.0 \pm 24\,(E/D)}$$

e.g. for $E \sim 0.04\ cm^{-1}$, $D \sim 10\ cm^{-1}$ (cytochrome a_3 in cytochrome c oxidase)

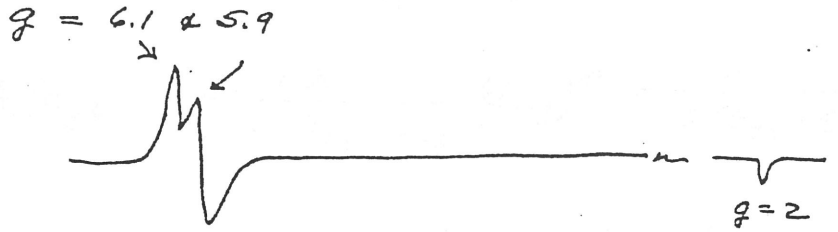

$E \sim 0.04\ cm^{-1}$ is a relatively small rhombic distortion.

(5) For low-spin heme, deviation of g-values from 2.0023 arises from spin-orbit interaction

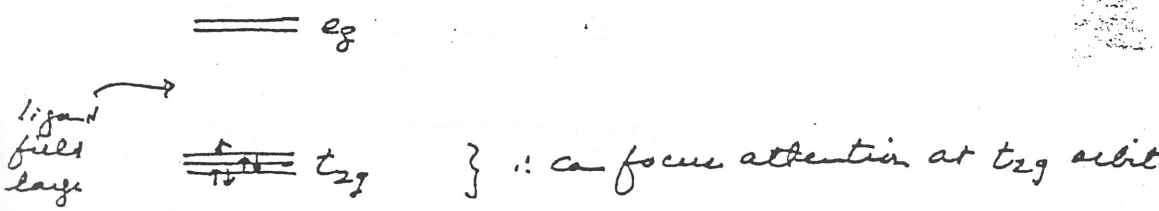

At this level of approximation, problem is orbitally degenerate

$\Rightarrow$ Jahn-Teller distortion to D_{2h} symmetry, which lifts degeneracy of 3 t_{2g} orbitals

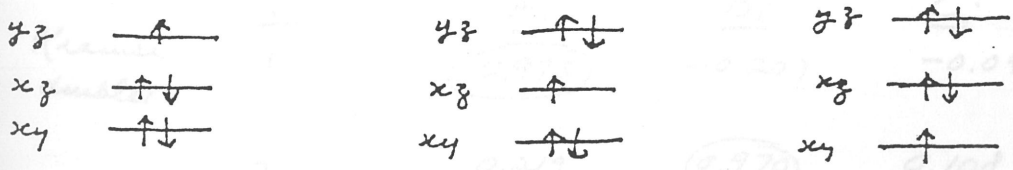

ground state	1st excited state	2nd excited state
$(d_{yz})^+$	$(d_{xz})^+$	$(d_{xy})^+$ ← spin "up"

Spin-orbit interaction mixes these states

For example,

$$\Psi_1^+ = A_1 (d_{yz})^+ + B_1(i)(d_{xz})^+ + C_1(d_{xy})^-$$

& $$\Psi_1^- = -A_1 (d_{yz})^- + B_1(i)(d_{xz})^- + C_1(d_{xy})^+$$

more explicitly

$$\Psi_1^+ = A_1(d_{yz})^+ + \frac{\langle d_{xz}^+ | -\lambda \vec{L}\vec{S} | d_{yz}^+ \rangle}{\epsilon_{yz} - \epsilon_{xz}} (d_{xz})^+ + \frac{\langle d_{xy}^- | -\lambda \vec{L}\vec{S} | d_{yz}^+ \rangle}{\epsilon_{yz} - \epsilon_{xy}} (d_{xy})^-$$

$$= A_1(d_{yz})^+ + \frac{i\lambda}{2(\epsilon_{yz} - \epsilon_{xz})} (d_{xz})^+ + \frac{\lambda}{2(\epsilon_{yz} - \epsilon_{xy})} (d_{xy})^-$$

where $\epsilon_{yz}, \epsilon_{xz}, \epsilon_{xy}$ are the energies of $(d_{yz})^\pm$, $(d_{xz})^\pm$, $(d_{xy})^\pm$

the so-called "hole" states

ϵ_{xy} ——— $(d_{xy})^\pm$

ϵ_{xz} ——— $(d_{xz})^\pm$

ϵ_{yz} ——— $(d_{yz})^\pm$

Spin-orbit interaction mixes these "hole" states

Similar final wavefunctions can be written for remaining two Kramer doublets

For azidoferrihemoglobin ($Hb \cdot N_3$), where $g_1 = 2.80$, $g_2 = 2.22$ and $g_3 = 1.72$

Kramer doublet	i	A_i	B_i	C_i	
	1	(0.973)	−0.207	−0.097	$\sim (d_{yz})^\pm$
	2	0.219	(0.970)	0.108	$\sim (d_{xz})^\pm$
	3	0.071	−0.126	(0.990)	$\sim (d_{xy})^\pm$

To fit observed g-values for azido ferrihemoglobin, requires

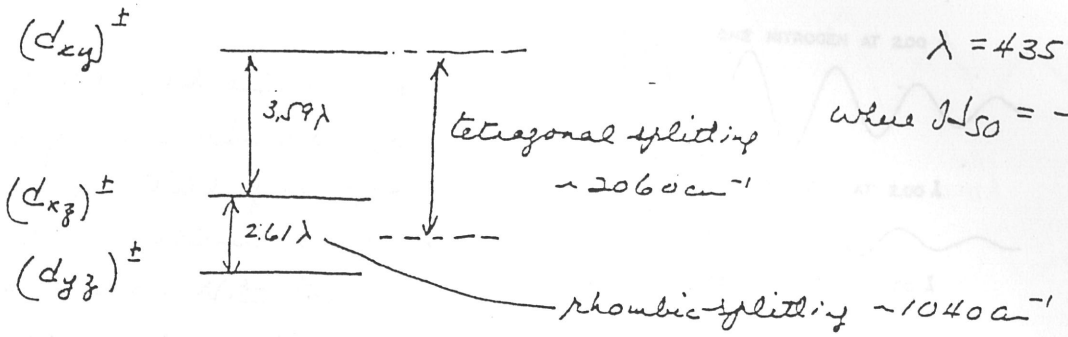

$\lambda = 435\ cm^{-1}$

where $\mathcal{H}_{SO} = -\lambda \vec{L} \cdot \vec{S}$

at 4.2 – 20 K, only $(d_{yz})^{\pm}$ Kramer doublet is populated!

Ref J. S. Griffith, "Theory of Transition-Metal Ion" Cambridge University Press

M. Kotani, Advances in Chem. Physics I, 159 (1964)

(6) Since different axial ligands affect the tetragonal and rhombic splittings differently, the g-values for a low-spin heme can be used to infer the axial ligands.

The relation between EPR parameters and structure of low spin ferric heme compounds (taken from [11])

Compound	Axial ligands		g values		
Glycera Hb $MeNH_2$	imid	RNH_2	3.30	1.98	1.20
Leg Hb pyridine	imid	pyr	3.26	2.10	0.82
Cytochrome c	imid°	met	3.07	2.26	1.25
Bis imid heme	imid°	imid°	3.02	2.24	1.51
Bis $imid^-$ heme	$imid^-$	$imid^-$	2.80	2.26	1.72
MbOH	$imid^-$	OH^-	2.55	2.17	1.85
Cyt. $P\text{-}450_{cam}$	imid°	RS^-	2.45	2.26	1.92
Cyt. c oxidase	imid°	imid°	3.0	2.2	1.5

This approach was used to argue that cytochrome a in cytochrome c oxidase is six-coordinate with N from neutral imidazoles as axial ligands

A better approach to infer the axial ligands of hemes in hemoproteins is EXAFS.

EXAFS spectroscopy has provided the first direct, compelling evidence demonstrating that the proximal ligand to the heme in P-450 (in states 1–5) and chloroperoxidase (state 2 and 4) is a thiolate sulfur. Ref. S.P. Cramer, J. H. Dawson, K.O. Hodgson and L.P. Hager, J. Am. Chem. Soc 100, 7282 (1978)

We shall systematically illustrate here this concept

(1)

A single damped sine wave expected for an iron absorber with a single shell of nitrogen backscattering atoms at various fixed distances. Note that both the phase and amplitude of the sine wave changes as the distance of the scatterer (first shell) from the absorber varies

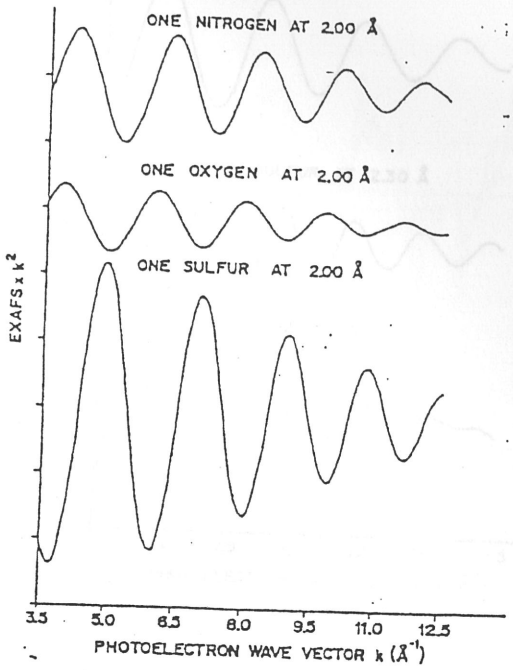

(2)

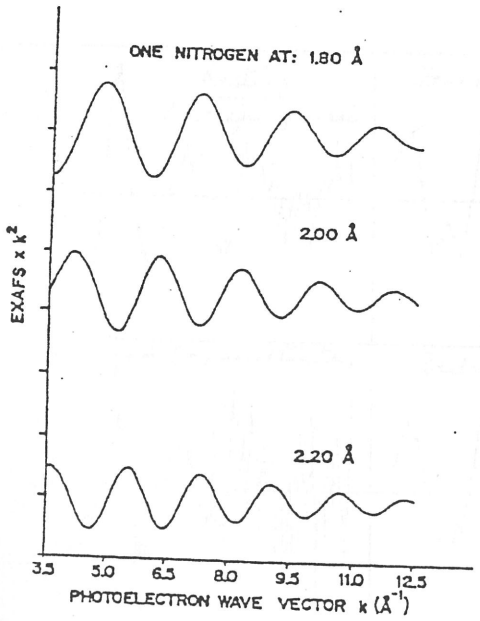

$\chi(k)\,k^2$ for a sulfur scatterer and iron absorber is dramatically different from that of oxygen or nitrogen scatterers with an iron absorber. The phase and amplitude of the EXAFS depends strongly on the type of backscattering atom, even when the interatomic distance is fixed. Sulfur is a stronger scatterer than N + O, so sulfur as a first shell atom from iron is easily identified. It is not possible, however, to distinguish oxygen from nitrogen

(3) EXAFS expected for five-coordinate heme iron with one sulfur as axial ligand

$k^2\chi(k)$ for an iron absorber with four first shell nitrogens @ 2.00Å and one first-shell sulfur at 2.30Å is a combination of the appropriate individual EXAFS sine waves of nitrogen and sulfur atoms. The sum begins to mimic what might be expected for the central iron of a porphyrin (coordination to four pyrrole nitrogens) with a single axial sulfur ligand.

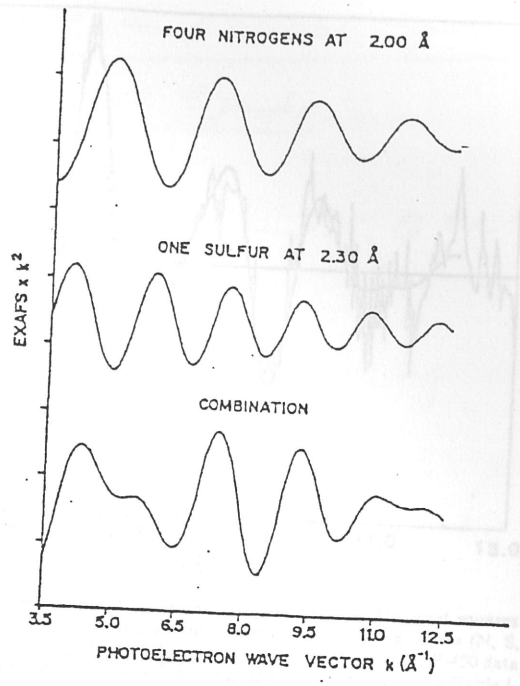

(4) Actual data (EXAFS) for various states of P-450 CAM

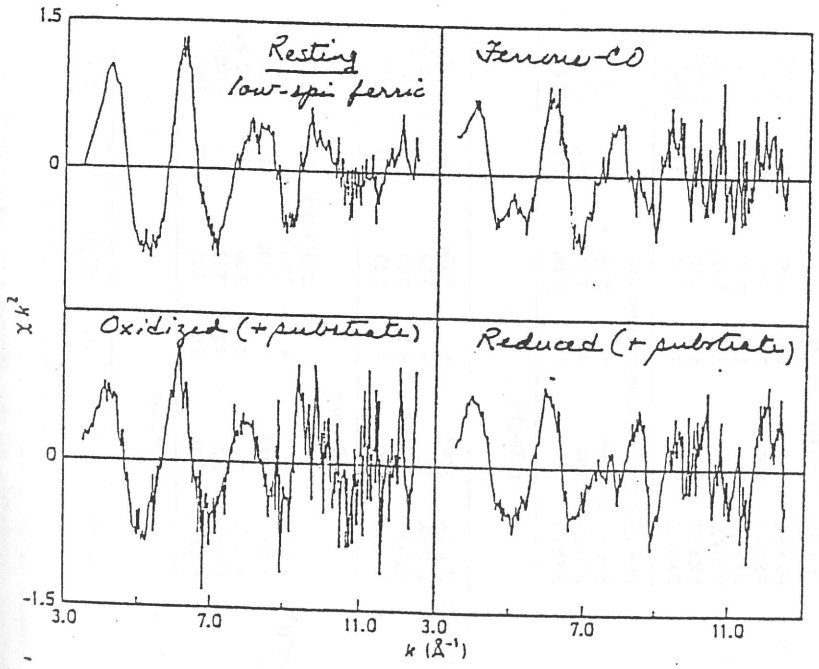

EXAFS spectra of P-450-CAM. The EXAFS spectra (weighted by k^2) for low-spin ferric, *1*, (*upper left*), high-spin ferric, *2*, (*lower left*), ferrous, *3*, (*upper right*), and ferrous carbonyl, *5*, (*lower right*) P-450-CAM.

Difference between (4N, 1S) combination and actual data result from additional backscattering from the carbon atoms on the ligands.

Table 1. Structural details for cytochrome P-450, chloroperoxidase, and relevant model complexes[a]

System	Method	Fe–N(porphyrin) R (Å)	Fe–N(porphyrin) N[b]	Fe–S(axial) R (Å)	Fe–S(axial) N[b]	Ref.
A. Ferric						
		Low-Spin				
P-450-CAM	EXAFS	2.00	5.0	2.22	0.6	[95]
P-450-LM2	EXAFS	2.00	4.8	2.19	0.8	[109]
P-450-CAM[c]	X-RAY	—	4	2.20	1	[96, 97]
$[Fe(TPP)(SC_6H_5)_2]^-$	X-RAY	2.008	4	2.336	1	[111]
$Fe(TPP)(HSC_6H_5)(SC_6H_5)$	X-RAY	—	4	2.27(RS$^-$) 2.43(RSH)	1 1	[112]
		High-Spin				
P-450-CAM	EXAFS	2.06	5.2	2.23	0.8	[95]
Chloroperoxidase	EXAFS	2.05	4.2	2.30	0.9	[109]
P-450-CAM[d]	X-RAY	2.05	4	2.20	1	[97, 98]
$Fe(PPIXDME)(SC_6H_4NO_2)$	X-RAY	2.064	4	2.324	1	[113]
B. Ferrous						
		High-Spin				
P-450-CAM	EXAFS	2.08	3.0	2.34[e]	0.6	[95]
$Fe(OEP)(SPr)^-$	EXAFS	2.05	3.8	2,33	0.4[f]	[114]
$Fe(TPP)(SEt)^-$	X-RAY	2.096	4	2.360	1	[115]
		Low-Spin Carbon Monoxide Complex				
P-450-CAM	EXAFS	1.98	3.3	2.32	1.0	[95]
$Fe(OEP)(SPr)(CO)^-$	EXAFS	2.00	4.4	2.33	0.2[f]	[114]
$Fe(TPP)(SEt)(CO)^-$	X-RAY	1.993	4	2.352	1	[115]
Fe(OEP)(PrSH)(CO)	EXAFS	2.01	5.1	2.41	0.8	[114]
Fe(OEP)(THT)(CO)	EXAFS	2.00	5.2	2.41	0.4[f]	[114]
Fe(OEP)(MeSSMe)(CO)	EXAFS	2.03	5.9	2.40	0.7	[114]
		Low-Spin Dioxygen Complex				
P-450-CAM[g]	EXAFS	2.00	7.8[h]	2.37	1.3	[116]
Chloroperoxidase[i]	EXAFS	2.00	7.4[h]	2.37	1.4	[116]
$[Fe(TpPP)(SC_6HF_4)(O_2)^-]^k$	X-RAY	1.990	4	2.369	1	[117]
$Fe(TpPP)(THT)(O_2)^m$	X-RAY	1.99–2.00	4	2.49	1	[118]

[a] EXAFS data were obtained by curve fitting. Abbreviations: TPP, tetraphenylporphyrin; PPIXDME, protoporphyrin IX dimethyl ester. OEP, octaethylporphyrin; SPr, n-propanethiolate; SEt, ethanethiolate; PrSH, n-propanethiol; THT, tetrathiophene; MeSSMe, dimethyldisulfide; TpPP, *meso*-tetrakis (α,α,α,α-*o*-pivalamidophenyl)porphyrin;
[b] The number (N) of atoms at the distance indicated;
[c] Data at 2.2 Å resolution. The iron is found to be 0.29 Å out of the plane of the four pyrrole nitrogen atoms toward the cysteinate axial ligand. The sixth ligand was found to be water (or hydroxide);
[d] Data at 1.7 Å resolution. The iron is found to be 0.43 Å out of the plane of the four pyrrole nitrogen atoms toward the cysteinate axial ligand. There is no sixth ligand. The $C_\beta S_\gamma Fe$ bond angle is 105.9°;
[e] Best fit to filtered EXAFS data. Fe–S_{ax} = 2.38 Å when unfiltered EXAFS data were analyzed;
[f] Analysis of solution data using parameters derived from the solid-state EXAFS of structurally defined model complexes may result in low values for N(S_{ax}) due to Debye-Waller effects (see Ref. 114);
[g] Fe–O(dioxygen) = 1.78 Å; N(O_{ax}) = 1.1;
[h] Analysis of low temperature data using parameters derived from the study of model complexes at room temperature may result in high N values due to Debye-Waller effects (see Ref. 116);
[i] Fe–O(dioxygen) = 1.77 Å; N(O_{ax}) = 1.3;
[k] Fe–O(dioxygen) = 1.818 Å;

Curve fitting of EXAFS result for resting (low-spin ferric) P-450 CAM

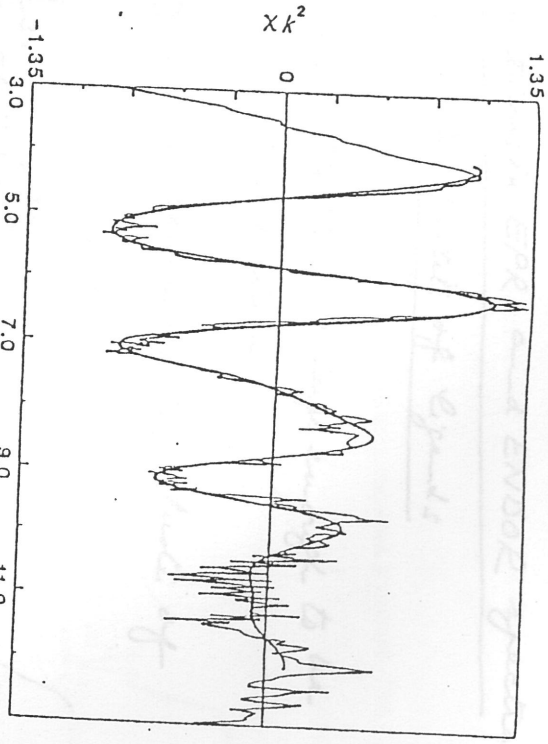

Curve-fitting result for the EXAFS data of low-spin ferric P-450-CAM. The least squares fit (dark line) to the measured data (light line) for structure determination. Three waves (N, S, C[α, *meso*]) were used. Fitting was over a range of k = 4–12 Å^{-1}. The best fits to the other P-450 data were qualitatively similar. Numerical results of all P-450 curve fittings are summarized in Table 1.

(5) Summary of structural results for cytochrome P-450 CAM & chloroperoxidase

Ligand Superhyperfine Interactions in EPR and ENDOR spectra provide some direct evidence of identity of ligands

(1) When ligand superhyperfine structure is large enough to be resolved in conventional EPR spectrum.

Illustrate this by way of the cytochrome a_3, Cu_B cluster of cytochrome c oxidase.

(a) Oxidized Cluster

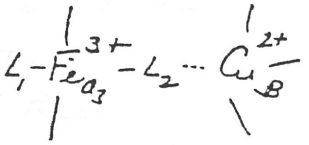

high-spin $S = 5/2$ $S = 1/2$ } Antiferromagnetic coupling $\Rightarrow S = 2$

if $L_2 = H_2O, F^-$, formate

No Conventional EPR!

low spin $S = 1/2$ $S = 1/2$ } $S = 0$ antiferromagnetic or 1 ferromagnetic

if $L_2 = OH^-, CN^-$

(b) Reduced Cluster

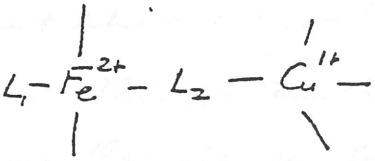

high-spin $S = 2$

if $L_2 = H_2O$

No Conventional EPR!

low spin $S = 0$.

if $L_2 = CO, NO$,

No EPR for CO complex; but NO is paramagnetic, so although NO-binding can convert Fe to low spin ($S = 0$), the nitrosyl heme is an odd electron system with $S = 1/2$

(c) EPR spectrum of ^{14}NO- and ^{15}NO adducts of reduced cytochrome $\underline{c}$ oxidase

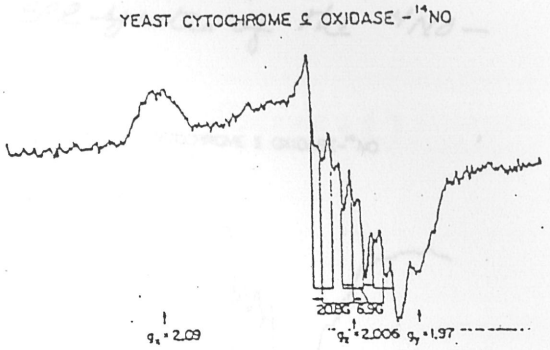

→ All 3 g-components are resolved ($g_1 = 2.09$; $g_2 = 2.006$; $g_3 = 1.97$)

→ The $g = 2.006$ component exhibits a (^{14}NO-adduct) nine-line hyperfine pattern, which can be interpreted in terms of the superposition of three sets of three lines arising from two nonequivalent nitrogens ($I=1$) interacting with the unpaired electron. The larger of the two hyperfine coupling constants is 20.8 Gauss and the smaller 6.9 Gauss.

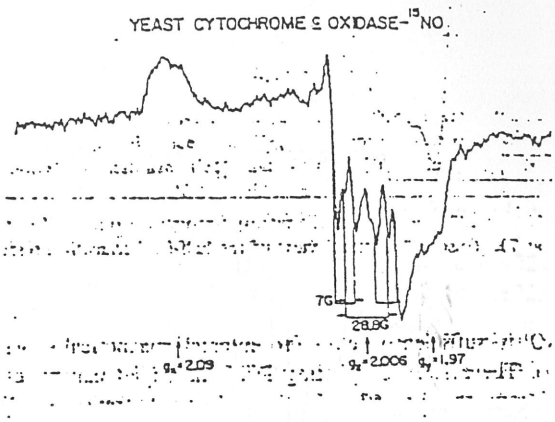

$\underline{^{15}NO\text{-adduct}}$: When ^{15}NO is used in the experiment, the ^{15}NO-bound protein exhibits an EPR spectrum with g-value identical to those of the ^{14}NO-bound species, but the $g = 2.006$ component shows a hyperfine pattern consisting of two sets of three lines. This pattern is consistent with the presence of one ^{14}N and one ^{15}N nitrogen bound axially to cytochrome a_3 with a 28.2 Gauss splitting for the ^{15}N and a 7.0 G splitting for the ^{14}N ligand.

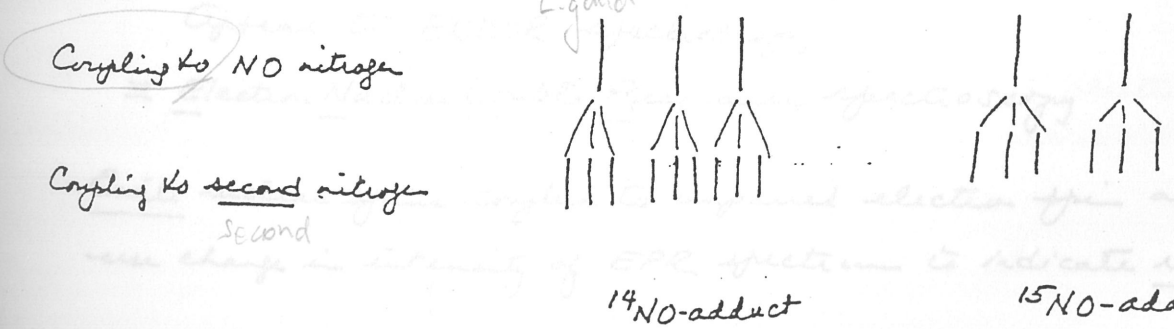

→ When experiments were repeated on a yeast cytochrome c oxidase preparation wherein all the histidines substituted with ^{15}N at both imidazole ring positions, the EPR spectra of the ^{14}NO- and ^{15}NO-adducts are altered.

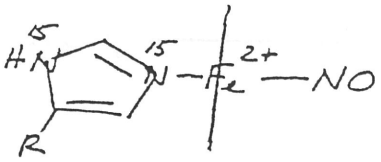

The EPR spectrum of the ^{15}NO-adduct of the (^{15}N) His protein consists of two sets of doublets, with a ^{15}NO nitrogen splitting of 27.5 Gauss and a splitting of 12 Gauss for the ^{15}N nitrogen of the histidine. The ^{14}NO-adduct exhibits a pattern consisting of 3 sets of doublets, with splitting of 31 Gauss x 10.1 G for the ^{14}NO and histidine ^{15}N nitrogen respectively.

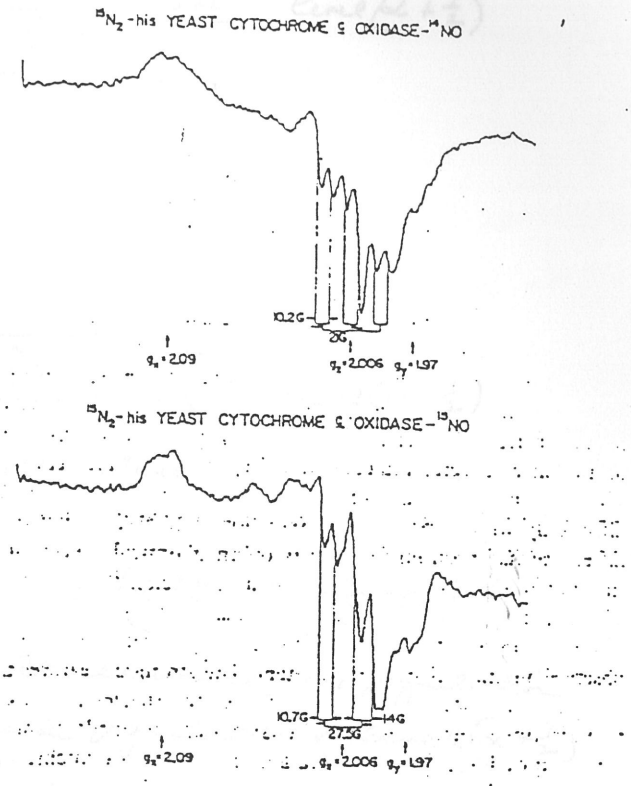

[redacted]. EPR spectra of the ^{14}NO and ^{13}NO complexes of reduced native and (^{15}N)His yeast cytochrome c oxidase. Frequency, 9.2 GHz; temperature, 30 K.

→ These experiments provide unequivocal identification of histidine as the endogenous fifth ligand to cytochrome a_3 (in the reduced state).

(2) When ligand superhyperfine interaction is too small to be resolved in EPR spectrum

Appeal to ENDOR spectroscopy

≡ Electron Nuclear Double Resonance spectroscopy

Excite nuclear spins coupled to unpaired electron spin and use change in intensity of EPR spectrum to indicate resonance

a) $\underline{I = \frac{1}{2}}$ nucleus coupled to electron spin

Energy level diagram

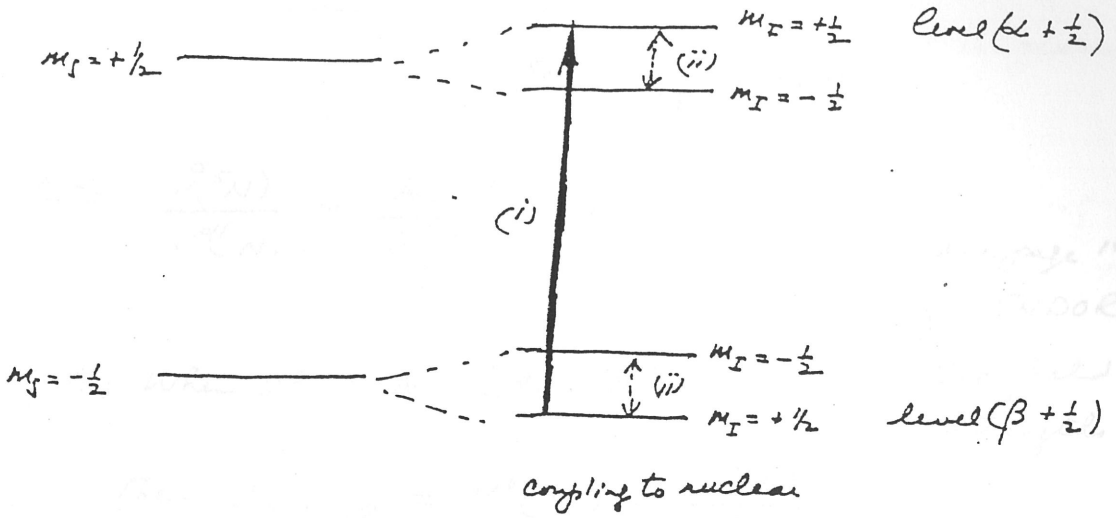

coupling to nuclear

(i) Saturate one of EPR transitions (EPR intensity = 0)

(ii) Slowly vary NMR frequency. At resonance, the population of level $(\beta + \frac{1}{2})$ will decrease, and population of level $(\alpha + \frac{1}{2})$ will increase. EPR will no longer be saturated and EPR intensity $\neq 0$.

(iii) The first order ENDOR spectrum of a nucleus of type I consists of transitions at frequencies given by:

(a) $\underline{\text{When } \nu^0 = \text{NMR Larmor frequency} < A}$

$$\nu_{ENDOR} = \frac{A}{2} \pm \nu^0$$

e.g. $\underline{^{14}N}$: a Larmor-split doublet centered at $\frac{A(^{14}N)}{2}$ split by $2\nu^0(^{14}N)$ (further splitting by electric quadrupole interaction)

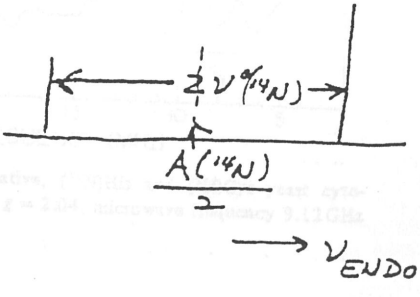

^{15}N: a Larmor-split doublet centered at $A(^{15}N)/2$ and split by $2\nu^0(^{15}N)$.

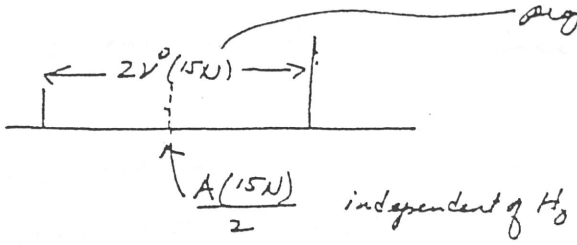

Note $\dfrac{\nu^0(^{15}N)}{\nu^0(^{14}N)} = \dfrac{A(^{15}N)}{A(^{14}N)} = 1.403$

see page 14 for ENDOR at two field strengths

(b) When $\nu^0 > A$ (e.g. ^1H)

Then $\nu_{ENDOR} = \nu^0(^1H) \pm \dfrac{A(^1H)}{2}$

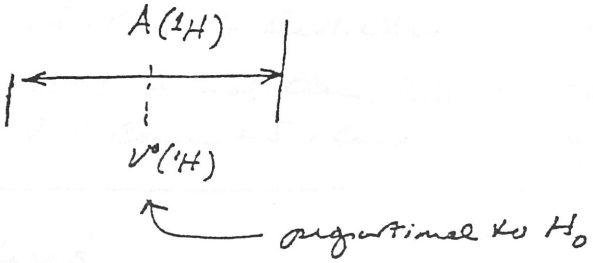

(c) ^1H, ^{14}N and ^{15}N ENDOR of Cu_A site of cytochrome c oxidase

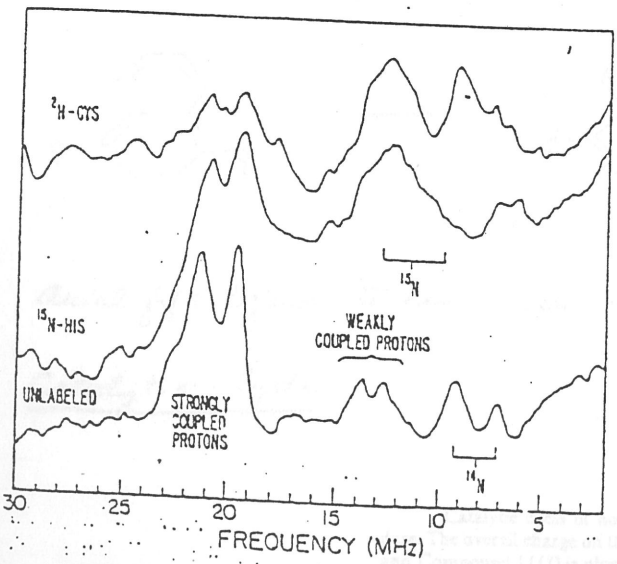

ENDOR spectra of native, (^{15}N)His and (^2H)Cys yeast cytochrome c oxidase observed at $g = 2.04$, microwave frequency 9.12 GHz and temperature 2.1 K.

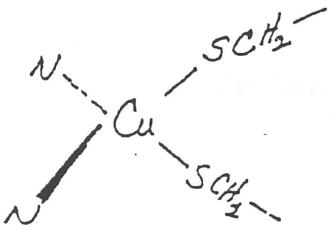

"Cu_A site"

In the ENDOR of the Cu_A site, there are NMR signals assignable to ^{14}N, weakly-coupled protons, and strongly coupled protons for native yeast cytochrome c oxidase.

→ ^{14}N signals is replaced by ^{15}N when the yeast is grown on ^{15}N-substituted (ring) histidine (98%)

→ Strongly coupled protons disappear or attenuated in intensity when the yeast is grown on deuterated cysteine with 2H (>90%) at the β-carbon (β-methylene)

→ These results provide unambiguous evidence for histidine and cysteine as ligands to Cu_A.

Ref: D. F. Blair et al Chemica Scripta 21, 43-53 (1983);
T. H. Stevens & S. I Chan, J. Biol. Chem 256, 1069 (1981);
T. H. Stevens et al, J. Biol. Chem. 257, 12106 (1982)
T. H. Stevens, D. F, Bocian & S. I Chan, FEBS 97, 314 (1979)

Return to Peroxidases

Horse-radish peroxidase (HRP)

2e⁻ oxidation

- Axial fifth ligand to heme iron is a nitrogen donor (histidine)
- Catalytic Cycle

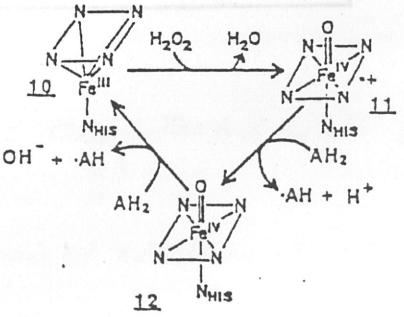

Catalytic cycle of horseradish peroxidase. The overall charge on the resting state *10* and Compound I (*11*) is plus one (the dot and the positive charge on *11* indicate the radical state and electron deficiency of the π electron system of the porphyrin ring), while Compound II (*12*) is neutral. Adapted from Ref. [20]

ENDOR of Cu_A site at two magnetic field strengths (14)

A: 3200 Gauss B: ~10,000 Gauss

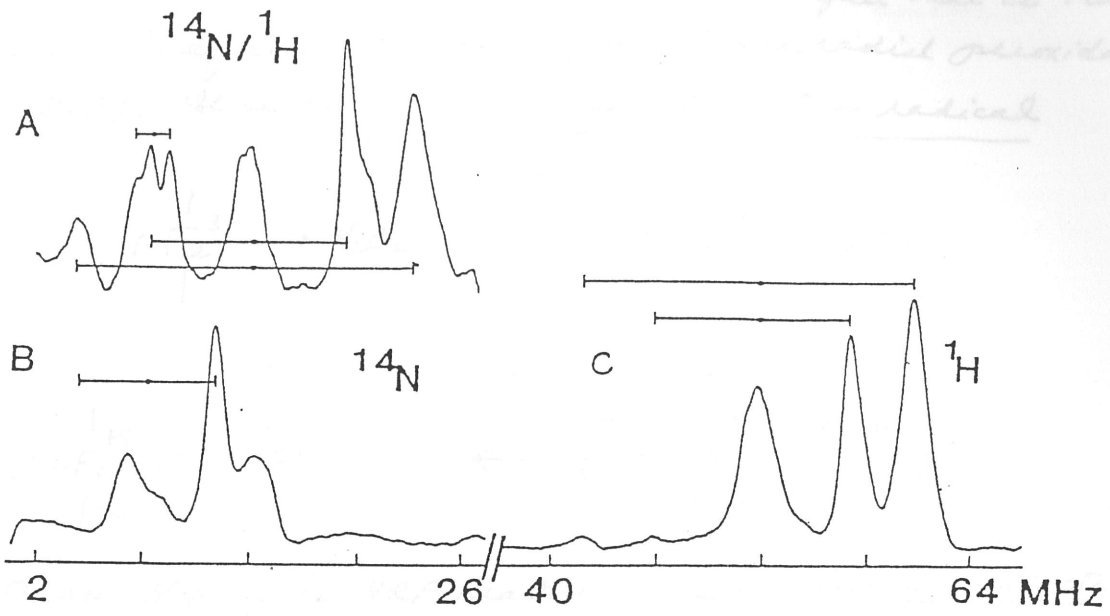

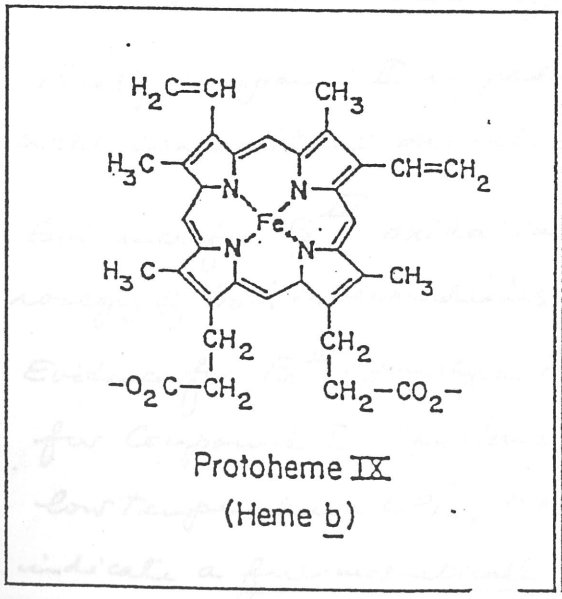

Protoheme IX
(Heme b)

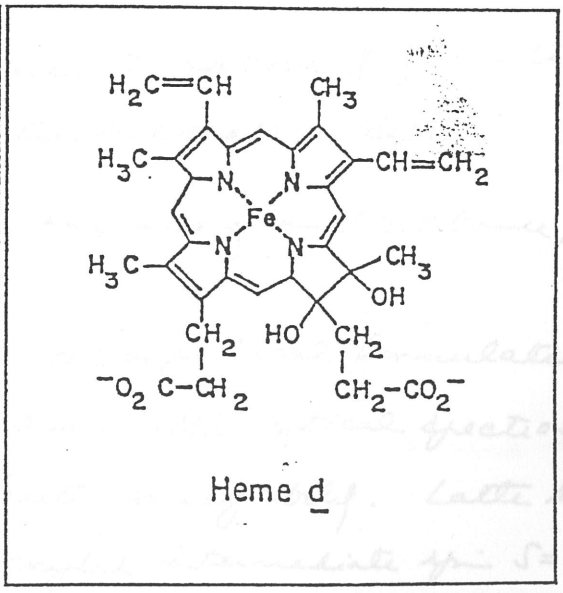

Heme d

→ The catalytic cycle begins with oxidation of the high-spin pentacoordinate ferric native enzyme by H_2O_2 to form a semi-stable intermediate called Compound I.

→ Compound I is a high-valent oxo-iron complex that is two oxidation equivalents above ferric horseradish peroxidase (HRP). It is an Fe(IV) porphyrin π-cation radical

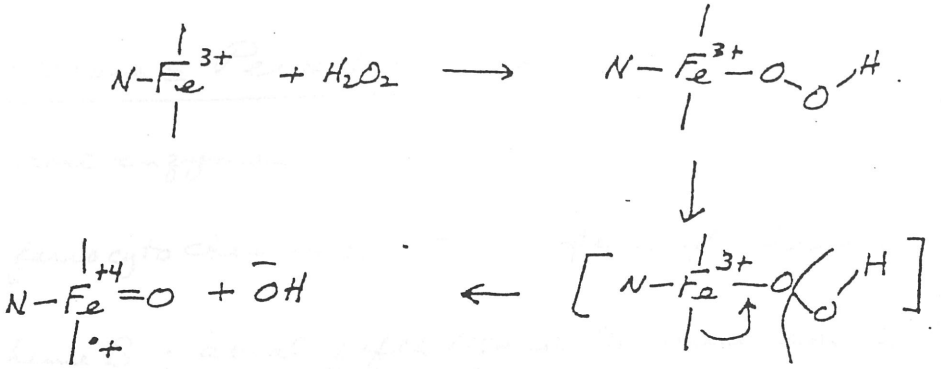

→ The next step of the HRP reaction cycle involves one-electron reduction of Compound I by organic substrate. This produces a second intermediate called Compound II, where the porphyrin is returned to the original state, but the iron is still Fe^{IV}, one oxidation equivalent above ferric state.

→ Finally, Compound II is reduced to native ferric state with concomitant one-electron substrate oxidation

→ Evidence for Fe^{IV} oxidation has come from Mössbauer spectroscopy of both intermediates

→ Evidence for Fe^{IV}-porphyrin π-cation radical formulation for Compound I has come from NMR, optical spectroscopy, low temperature EPR, magnetic susceptibility. Latter studies indicate a ferromagnetically coupled intermediate spin S=1 Fe^{IV} and a porphyrin π-radical cation

→ EXAFS provides evidence for high-valent oxo intermediate for both Compounds I and II

→ Resonance Raman } data indicate that unpaired electron is in
ENDOR

an a_{1u} Molecular orbital, so the complex has $^2A_{1u}$ ground state

→ Recent work by Ortiz de Montellano & coworkers strongly suggests that the substrate oxidation reaction takes place at the heme edge, not at the heme pocket containing the oxo-ferryl group.

Cytochrome c Peroxidase (CcP)

- Yeast enzyme
- ferrocytochrome c ⟶ ferricytochrome c
- heme B; axial fifth ligand to heme iron is a nitrogen from histidine.
- Catalytic cycle

$$CCP + H_2O_2 \rightarrow CCP\ Compound\ I + H_2O$$

$$CCP\ Compound\ I + Cyt\text{-}c[Fe^{II}] + H^+ \rightarrow CCP\ Compound\ II + Cyt\text{-}c[Fe^{III}]$$

$$CCP\ Compound\ II + Cyt\text{-}c[Fe^{II}] + H^+ \rightarrow CCP + Cyt\text{-}c[Fe^{III}] + H_2O$$

- CcP Compound I differs from HRP Compound I in that the radical cation is located on a tryptophan, not the porphyrin
- Crystal structures of CcP and CcP·Cyt.c complex are known. That of the CcP·cyt.c complex just appeared.

Catalases

- catalyzes disproportion of $2H_2O_2 \longrightarrow O_2 + 2H_2O$
- Most catalases have iron protoporphyrin IX as the prosthetic

group and axial tyrosinate ligation. However, both the catalase from Neurospora crassa and HP II catalase from E. coli have iron chlorins as prosthetic group.

↘ see p. 14 for a comparison of Chlorin (heme d) vs heme B.

- Catalytic cycle

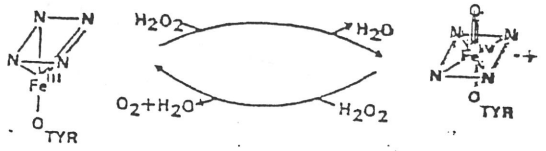

13 14

Catalytic cycle of catalase. The resting state *13* and Compound I (*14*) are neutral (the dot and the positive charge on *14* indicate the radical state and electron deficiency of the π electron system of the porphyrin ring)

→ Reaction cycle begins with high-spin ferric state, which reacts with a molecule of H_2O_2 to form Compound I.

→ Next, oxidation of a second H_2O_2 yields O_2, with concomitant return of catalase Compound I to the native resting state.

EXAFS of High-Valent Oxo-Iron Porphyrin Systems

Best evidence for $Fe^{IV}=O$ in Compound I and II intermediates formed during the catalytic cycle has come from EXAFS and Raman spectroscopy

- $Fe^{IV}=O$ bond ~ 1.6-1.7 Å
- $Fe^{IV}=O$ stretching frequency ~ 788 cm^{-1}, which is sensitive to $^{16}O/^{18}O$ and pH (weak H-bond). ($< 15\ cm^{-1}$)

$$Fe^{IV}=O \cdots H-B$$

Raman Spectroscopy

Raman spectroscopy involves a light scattering experiment in which the frequency of the scattered light is analyzed. Most of the light emerges at the incident frequency

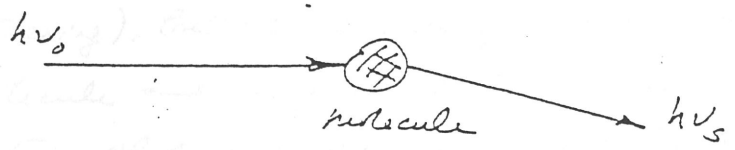

elastic : $\nu_s = \nu_0$

inelastic : $\nu_s = \nu_0 - \frac{E_f - E_i}{h}$

where E_i and E_f denote the energies of the molecule before and after the scattering process.

(Rayleigh scattering), but occasionally a photon scatters inelastically from a molecule and is shifted from its original frequency by a quantum of energy corresponding to a molecular transition of the system. The transition may be translational (e.g. lattice modes of a crystal), rotational, vibrational. In this course, we are concerned with vibrational Raman spectroscopy only.

A photon can lose energy by exciting a molecule to an excited vibrational state, or gain energy by inducing the reverse process, producing Stokes or anti-Stokes lines, respectively, in the Raman spectrum.

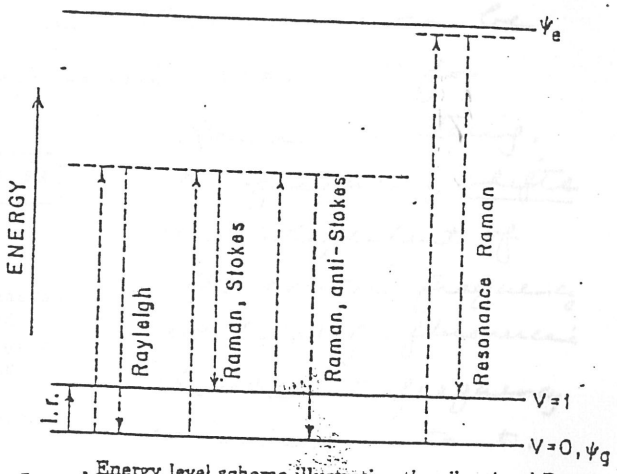

Energy level scheme illustrating the vibrational Raman scattering process.

Resonance Raman spectroscopy obtains when one tunes the frequency of the incident light to approach that of an electronic transition. Resonance enhancement of the Raman bands occurs. Often times, this enhancement is $\sim 10^6$. So biophysical chemists exploit this resonance enhancement to home in on the vibrations of a biological chromophore. By exciting only the chromophore in the biological macromolecule, one preferentially enhances the Raman vibrational bands associated with the chromophore and selects out these bands from the myriad vibrations of the whole molecule.

With modern tunable lasers this kind of spectroscopy is relatively easy to accomplish.

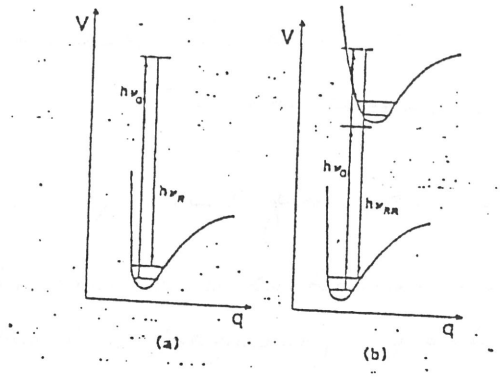

Diagrams of potential energy, V, versus internuclear separation, q, for a molecule undergoing vibrational excitation by (a) the Raman effect or (b) a resonance Raman effect ($h\nu_0 = h\nu_e$) or a pre-resonance effect ($h\nu_0 < h\nu_e$).

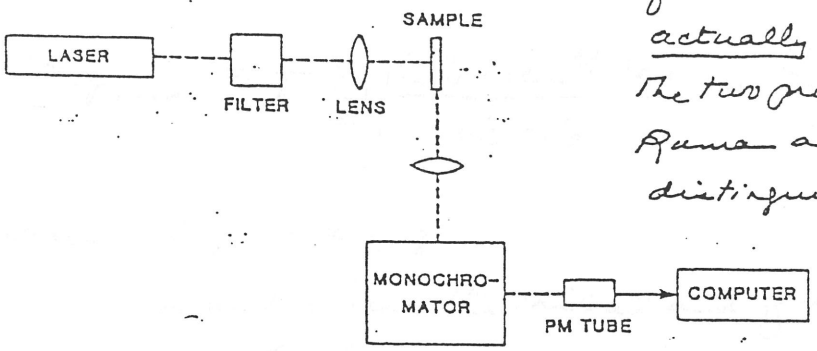

Experimental set-up for Raman spectroscopy. The desired laser line is isolated from other plasma lines by a narrow bandpass filter or broadband prism monochromator, then focused onto a sample in a capillary tube. A collecting lens placed at a 90° angle to the incident beam focuses the scattered light onto the entrance slit of a monochromator with output to a photomultiplier tube (in the case of a scanning instrument) or a diode array detector.

Note under resonance conditions, there is frequently interference from fluorescence. Here, the photon is actually absorbed & reemitted. The two processes, namely resonance Raman and fluorescence can be distinguished because (1) for Raman scattering, the frequency shifts are independent of the exciting frequency while (2) for fluorescence the absolute frequency remains constant.

Moreover, for liquids, fluorescence almost always occurs in a broad spectral band, while Raman bands are sharp. An approach to reduce interference from fluorescence is to exploit the short lifetime of fluorescence ($< 10^{-9}$ sec) and time-resolve the emitted light using pulsed laser sources. Fortunately, many biological chromophores have low fluorescence yields due to effective quenching mechanisms.

- Raman intensities

$$I = \frac{2^7 \pi^5}{3^2 c^4} I_0 \nu_s^4 \sum_{i,j} |d_{ij}|^2$$

where I_0 is the intensity of the incident light, $\nu_s \equiv$ its frequency

of the scattered light, and α_{ij} is an element of the scattering tensor $\underline{\alpha} = \begin{pmatrix} \alpha_{xx} & \alpha_{xy} & \alpha_{xz} \\ \alpha_{yx} & \alpha_{yy} & \alpha_{yz} \\ \alpha_{zx} & \alpha_{zy} & \alpha_{zz} \end{pmatrix}$ x, y, z molecular axes

Actually, the derivatives with respect to nuclear displacement of the molecular polarizability, i.e., $\alpha_{ij} = \alpha_{ij}^{0} + \sum_k \frac{\partial \alpha_{ij}}{\partial q_k} q_k$ are important for Raman scattering.

The resonance enhancement of a Raman band comes about via the frequency dependence of the molecular polarizability According to Kramers-Heisenberg-Dirac dispersion equation

$$(\alpha_{ij})_{mn} = \frac{1}{h} \sum_e \left[\frac{(M_j)_{me}(M_i)_{en}}{\nu_e - \nu_0} + \frac{(M_i)_{me}(M_j)_{en}}{\nu_e + \nu_s} \right]$$

where $i, j \equiv x, y, z$

m and n are the initial and final states of the molecule

e is an excited electronic state and $\sum_e$ sums over all excited states

$(M_j)_{me}$ and $(M_i)_{en}$ are electric dipole transition moments, along the directions j and i, from m to e and from e to n.

$\nu_e \equiv$ frequency of the transition from m to e

$\nu_0, \nu_s \equiv$ frequency of the incident and scattered photons

As ν_0 approaches ν_e, α_{ij} is subject to pre-resonance enhancement through the first term in the above expression. Typically, one element of the summation dominates all others.

- Heme scattering

Dominant features of RR spectra of heme proteins arise from porphyrin ring modes in the 1000 – 1700 cm^{-1} region

Vibrations involving the iron atom are not strongly enhanced because $\pi - \pi^*$ transitions are largely localized on the porphyrin ring

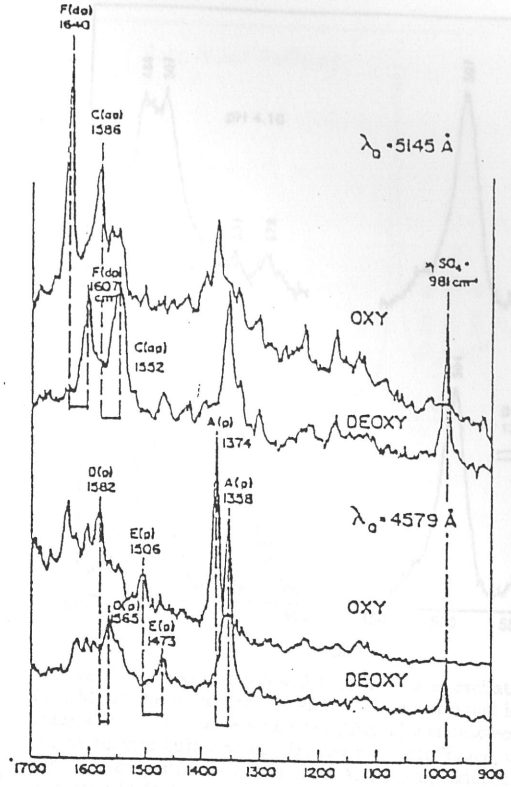

Figure 4. Resonance Raman spectra of oxy- and deoxyhemoglobin in the α–β (λ_0 5145 Å) and Soret (λ_0 4519 Å) scattering regions. The solutions were 0.68 and 0.34 m*M* in heme for oxy- and deoxyhemoglobin, respectively, and the latter contained 0.4 *M* $(NH_4)_2SO_4$, the $\nu_1(SO_4^{2-})$ band (981 cm^{-1}) of which is indicated. Frequency shifts for corresponding bands are marked by the arrows (from ref 17).

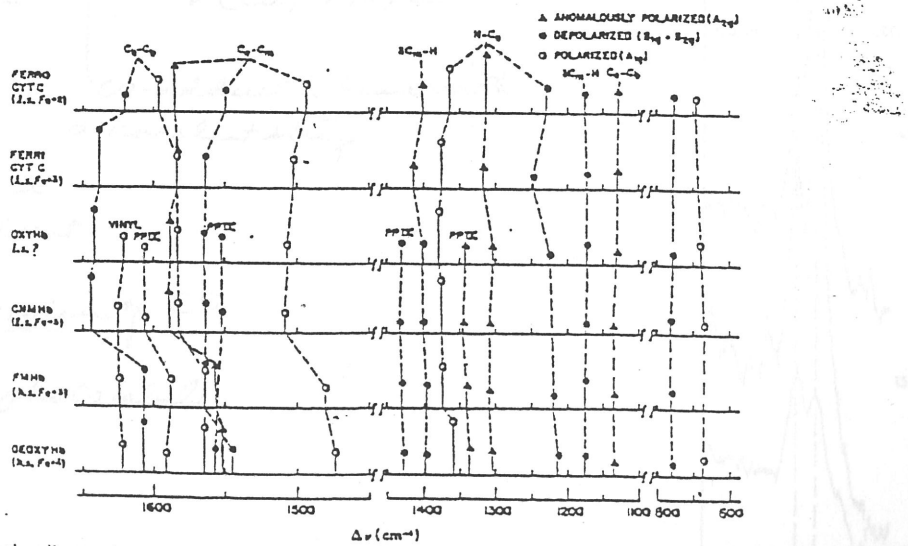

Figure 5. Correlation diagram for resonance Raman bands of hemoglobin and cytochrome c. Spin and oxidation states of the various species are indicated. See text for discussion of the oxyhemoglobin oxidation state. The lengths of the solid lines are roughly proportional to the observed relative intensities at 5145 Å excitation (4965 Å for FMHb) for anomalously polarized (▲) and depolarized (●) bands, and at 4579 Å for polarized (○) bands. Suggested assignments (approximate) to various heme internal coordinates are indicated at the top. The bands marked PPIX (protoporphyrin) and VINYL are observed for hemoglobin derivatives only (from ref 17).

Oxidation state markers

Spin state markers

• Mb – CO

→ effect of protonation of distal histidine

– protonation removes steric hindrance to upright binding of CO

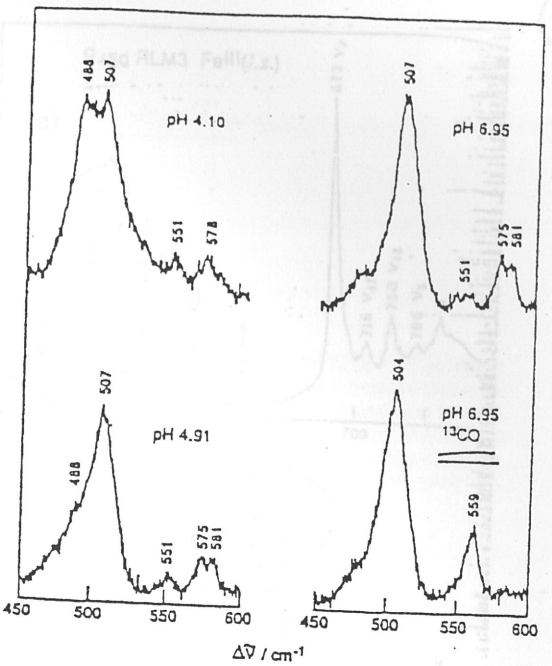

FIGURE 1: RR spectra with 413.1-nm Kr^+ laser excitation of MbCO (1 mM) at the indicated pH values. The last panel is of a sample made with ^{13}CO. Sperm whale Mb (Sigma) was dissolved in deaerated 0.1 M acetate buffer at the desired pH, centrifuged, deoxygenated for 30 min by stirring beneath an Ar stream, reduced with sodium dithionite (4-fold excess), and equilibrated by stirring under a stream of CO for 15 min. [^{13}CO was admitted to a vessel containing the reduced solution (free volume ~100 mL), which was stirred for 15 min.] Spectra were obtained in backscattering from spinning NMR tubes with a Spex 1401 double monochromator equipped with a cooled photomultiplier (RCA) and photon-counting electronics.

Table I: Protein and Analogue CO Adduct Vibrational Frequencies (cm^{-1})

species	ν(C–O)	ν(Fe–C)	ν(Fe–C)$_{calcd}$[a]	ref
Mb neutral pH	1947	507	505	b
Mb low pH	1967	488	490	b
FeSP-15 (N-MeIm)[c]	1945	506	506	d
FePPDME (ImH)[e]	1960	495	495	f

[a] Calculated from the observed ν(C–O) by using eq 1. [b] This work and Fuchsman and Appleby (1979). [c] Heme with intermediate length "strap", *N*-methylimidazole complex in benzene/methylene chloride (Yu et al., 1983). [d] Yu et al. (1983). [e] Iron(II) protoporphyrin dimethyl ester, imidazole complex in methylene chloride (Evangelista-Kirkup et al., 1986). [f] Evangelista-Kirkup et al. (1986).

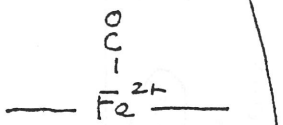

low pH

ν(Fe–C) 488 cm^{-1}

ν(CO) 1967 cm^{-1}

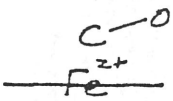

high pH

ν(Fe–C) 507 cm^{-1}

ν(CO) 1947 cm^{-1}

protein-free CO-imidazole adduct of protoheme in a non-polar solvent

CO-adduct to heme with a covalent strap

→ Photodissociation of CO

Mb–CO is photolabile

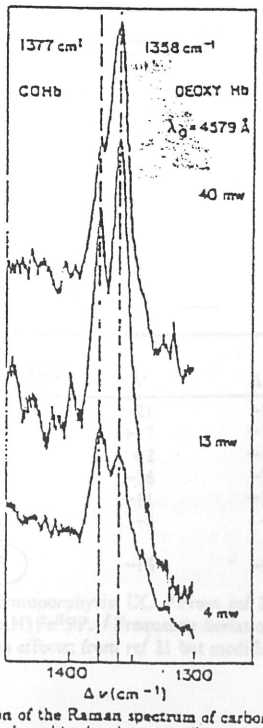

Figure 6. Portion of the Raman spectrum of carbonmonoxyhemoglobin (1377-cm^{-1} peak), showing reversible photodissociation to deoxyhemoglobin (1358-cm^{-1} peak). The sample, 0.66 mM COHb with sodium dithionite added, was placed under argon and run in a (sealed) rotating cell, at ~2000 rpm. The changing peak heights correspond to changing ratios of COHb and deoxyHb at the indicated power levels (measured at the sample) of 4579-Å Ar^+ laser radiation. The spectra were recorded in order *of decreasing* power levels, and the absorption spectrum of the solution at the end of the experiment corresponded to that of pure COHb. Photodissociation is less pronounced with longer wavelength excitation (from ref 17).

• Cytochrome P450 (microsomes)

RR evidence for Thiolate coordination

Low frequency (a) & high frequency (b) RR spectra of P450

Fe^{III} – S stretch ~ 350 cm^{-1}

first reported by Champion for P-450cam (Pseudomonas putida)

JACS 104, 5469-5472

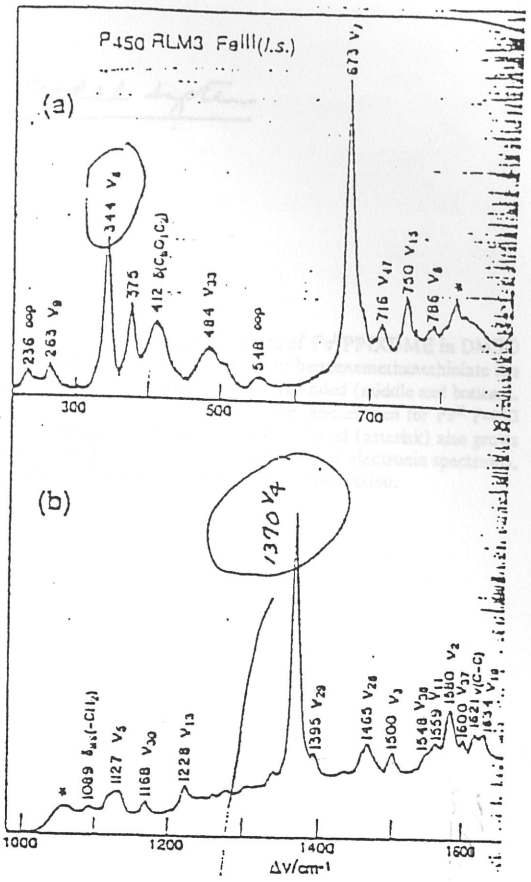

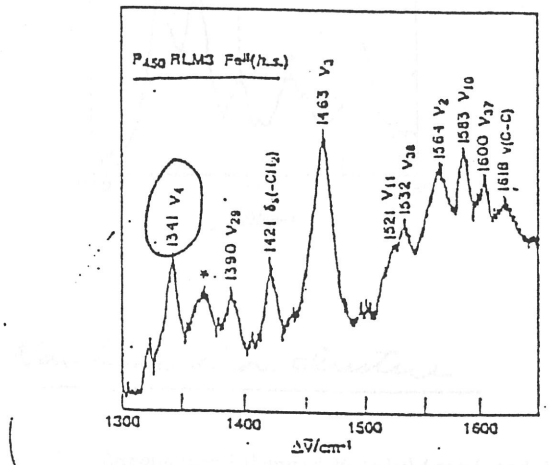

ν_4 (Fe^{III}–Im$_2$) 1373 cm^{-1}

ν_4 (Fe^{II}–Im) 1357 cm^{-1}

Porphyrin Marker Band Frequencies (cm^{-1}) for P-450 RLM3 and Model Compounds

band freq						
Fe^{III} P-450[a]	$(ImH)_2Fe^{III}PP$[c]	$(DMSO)(RS^-)Fe^{III}PP$[c]	Fe^{II} P-450[a,b]	(2-MeImH)$Fe^{II}PP$[c]	Δ[e]	Δ[f]
1634	1640	1637	1583	1604	−21	−13
1600	1602		1600	1583	+17	+12
1580	1579	1579	1564	1562	+2	+10
1559	1562		1521	1547	−26	−20
1548	1554		1532	1521	+11	+20
1500	1502	1500	1463	1471	−8	−1
1465	1469					0
1370	1373	1373	1341	1357	−16	−17

[a] ref 15. [b] Present work. [c] From ref 21; ImH = imidazole, 2-MeImH = 2-methylimidazole, and PP = protoporphyrin IX. [d] From ref 22; DMSO = dimethyl sulfoxide and RS^- = p-nitrobenzenethiolate. [e] Frequency difference Fe^{II} P-450 minus (2-MeImH)Fe^{II}PP. [f] Frequency deviations of $(ImH)_2Fe^{II}PP$ from the value expected on the basis of the porphyrin core size, and attributed to π-back-donation effects; from ref 21 but modified according to the subsequent core size parameters in ref 41.

Taken from Spiro et al Inorg. Chem (1989) 28, 4491-4495

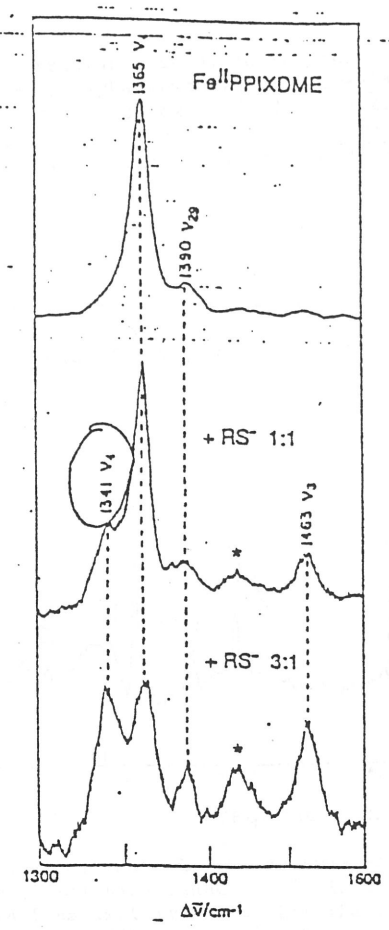

Model system

413.1-nm excited RR spectrum of Fe^{II}PPIXDME in DMSO (top) to which the indicated molar ratios of benzenemethanethiolate ion (prepared by NaH reaction with RSH) were added (middle and bottom). Growth of ν_3 and ν_4 bands at the same frequencies seen for Fe^{II} P-450 reflect thiolate adduct formation. A DMSO band (asterisk) also grows in, due to decreased solution absorbance (shifted electronic spectrum). Data acquisition: 0.5-cm^{-1} intervals; 3-s accumulation.

• Non-heme iron clusters

Table I. Resonance-Enhanced Metal-Ligand and Ligand Vibrational Modes in Metalloproteins[a]

Type of Binding	ν(M-L)	ν(Ligand)	Example
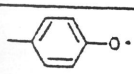	(575)	803, 869, 1164, 1281, 1497, 1597	Purple acid phosphatase[c]
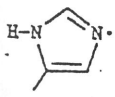	245	1140, 1168, 1256, 1330, 1426, 1490	Cu(ImH)$_4$Cl$_2$[d]
	225, 265	n.o.	Oxyhemocyanin[d]
HO···Fe	565	n.o.	Methemerythrin(OH)[e]
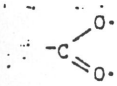	338	662	Fe$_2$O(Ac)$_2$(HBpz$_3$)$_2$[f]
	n.o.	(530)	Methemerythrin[g]
-CH$_2$-S···Fe	314, 348, 363, 376	653	Rubredoxin[h]
-CH$_2$-S···Cu	(373, 401, 409, 428)[b]	753	Azurin[i]

[a]Vibrational frequencies in cm^{-1}. ν(M-L) = metal-ligand stretching mode, ν(ligand) = internal ligand mode, n.o. = not observed. Values in parentheses are tentative assignments. [b]Coupled ν(Cu-S) + δ(Cys) modes. [c](14). [d](15). [e](16). [f](17). [g](18). [h](19). [i](20).

Figure 4. Structures of binuclear metal clusters. (a) Iron-oxo cluster in oxyhemerythrin from Themiste dyscrita; L denotes a coordinated hydroperoxide (27). (b) Iron-sulfur cluster in oxidized ferredoxin from Spirulina platensis (28). Starred ligands can be exchanged with appropriate species in solution.

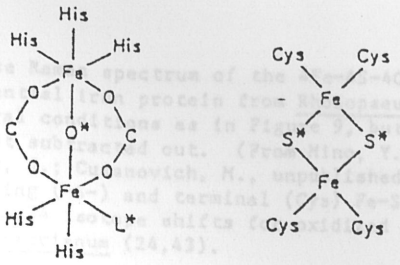

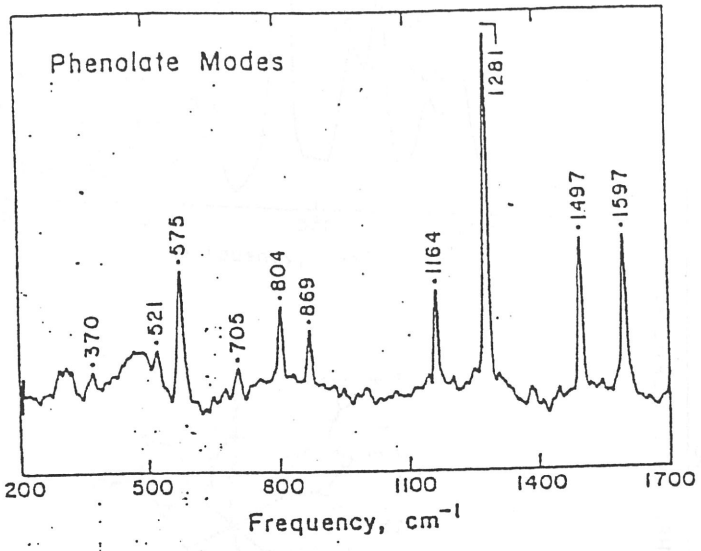

Figure 3. Resonance Raman spectrum of purple acid phosphatase. Protein (5 mM) maintained at 5°C in a glass Dewar and probed with 514.5 nm excitation (within the 560 nm phenolate → Fe(III) CT band, ε = 4,000 M^{-1} cm^{-1}). The broad, underlying feature from 400–550 cm^{-1} is due to Raman scattering from glass. (Reproduced from Ref. 14. Copyright 1987 American Chemical Society.)

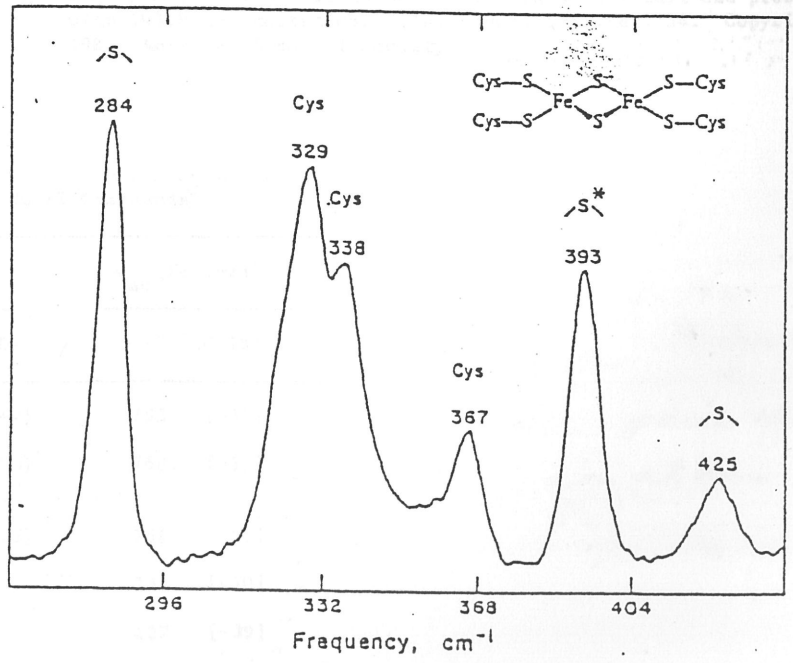

Figure 9. Resonance Raman spectrum of the 2Fe–2S–4Cys cluster in oxidized spinach ferredoxin. Protein (~2 mM) maintained at 15 K in a helium Displex and probed with 488.0 nm excitation. Spectral contribution of ice in 220–320 cm^{-1} region has been subtracted. (Data from Ref. 21). Starred features indicate